1 GENERAL

This alloy is a delta ferrite-free compositional modification of 17-4PH precipitation-hardening martensitic stainless steel containing less chromium and slightly higher nickel. Vacuum arc remelting lowers the alloy's gas content, reduces and disperses inclusions, and minimizes alloy segregation during solidification. These factors, coupled with the elimination of delta ferrite, result in superior transverse toughness compared to 17-4PH.

The alloy transforms to martensite on cooling to room temperature from the solution treatment. Hardening results from the precipitation of a copper-rich phase at temperatures of only 900 to 1150F, depending on the properties desired.

The corrosion resistance of this alloy is comparable to Type 304 in most media. Its oxidation resistance is superior to Type 410 but inferior to Type 430. The alloy is available as billet, plate, bar, and wire. It is forgeable, castable, weldable, and machinable.

Many physical and mechanical properties of this alloy are the same as for 17-4PH. Consequently, some of the data presented here were determined for 17-4PH and are noted as such. For properties which are independent of melting practice (air melt versus consumable electrode vacuum arc remelt), the melting method is usually not specified and the reader is to assume the data apply to either method.

1.1 Commercial Designation - 15-5PH precipitation-hardening stainless steel

1.2 Alternate Designations - UNS S15500; UNS J92110; AISI S15500

1.3 Specifications

1.3.1 *[Table]* AMS specifications for wrought products.

1.3.2 *[Table]* ASTM specifications for wrought products.

1.3.3 *[Table]* AMS specifications for investment castings.

1.3.4 *[Table]* AMS specifications for tubular centrifugal castings.

1.4 Composition

1.4.1 *[Table]* Specified composition for wrought products.

1.4.2 *[Table]* Producer's specified composition for castings.

1.4.3 *[Table]* AMS specified composition for investment castings.

1.4.4 *[Table]* AMS specified composition for tubular centrifugal castings.

1.4.5 *[Table]* AMS specified composition for weld electrodes and wire.

Fe	
15.0	Cr
4.50	Ni
0.30	Cb
3.5	Cu

1.5 Heat Treatment

1.5.1 Solution treat to Condition A, 1900 + 25F, 30 to 60 minutes, oil quench or air cool to below 90F (Refs. 1, 27).

1.5.2 *[Table]* Age Condition A to H Conditions (Precipitation hardening heat treatment schedules).

1.5.2.1 Precipitation in this alloy is complex. The formation and growth mechanisms of the several types of precipitates have been recently studied and described in detail in reference 54.

Aging produces a hardness peak at around 850F, followed by softening and then a second hardening beginning at about 1200F (see Figures 1.6.3 to 1.6.5). TEM observations reveal the successive formation (between 850 and 1200F) of two types of coherent precipitate, one type subsequently becoming partialy coherent rods with selective growth direction, the other partialy incoherent globules. All of the precipitates are enriched in copper. Aging beyond 1200F produces new precipitates which are coherent at first, and then become partially incoherent within the range 1350 to 1550F.

An earlier study (Ref. 53) also found the initial peak hardening on direct aging from the solution treatment, evidenced by resistivity (Figures 2.2.2.1 and 2.2.2.2) and hardness (Figure 1.6.6) measurements. A hardening peak was also observed during aging at a relatively lower temperature range (Between 780 and 890F) after higher temperature aging (1040 to 1110F) (see Figure 2.2.2.3). That peak corresponded to a severe drop in notch tensile strength (see Figure 3.2.7.1.3). The investigators attributed the hardening and attendant notch embrittlement to formation of a Ni-rich zone.

1.5.2.2 Precipitation hardening alloys are generally susceptible to hydrogen embrittlement. This susceptibility can be minimized by overaging or other treatments, or both, that alter the microstructure. One possible explanation of the beneficial effect of overaging is the development of incoherent precipitates, the interfaces of which act as hydrogen traps and alter the stress or strain induced localization of hydrogen.

Due to the fact that hydrogen diffusion is rapid compared to other interstitial atoms, and hydrogen is known to interact with defects and segregate to regions of localized lattice dilation, one may expect the aging kinetics and the resulting properties to be

This section produced with the support of NASA-Lewis Research Center.

altered if the process takes place in a hydrogen environment. These are demonstrated in Figures 1.5.2.2.1 through 1.5.2.2.6, which show two hardening reactions, one of which only develops during higher temperature aging at 900F and above. The presence of hydrogen increases peak hardness and decreases time to achieve peak hardness. Outgassing at room temperature of material aged in hydrogen increases hardness in most cases.

1.5.2.2.1 *[Figure]* Influence of hydrogen aging treatment environment on age hardening at 700F.

1.5.2.2.2 *[Figure]* Influence of hydrogen aging treatment environment on age hardening at 800F.

1.5.2.2.3 *[Figure]* Influence of hydrogen aging treatment environment on age hardening at 900F.

1.5.2.2.4 *[Figure]* Influence of hydrogen aging treatment environment on age hardening at 1000F.

1.5.2.2.5 *[Figure]* Influence of hydrogen aging treatment environment on age hardening at 1100F.

1.5.2.2.6 *[Figure]* Influence of hydrogen aging treatment environment on 900F aged tensile properties.

1.5.2.3 A dimensional change takes place on precipitation hardening.

1.5.2.3.1 *[Table]* Dimensional change (contraction) from hardening heat treatment.

1.6 Hardness

1.6.1 Producer's specified acceptable hardness and strength for Condition A, see Table 3.2.1.7.

1.6.2 Producer's specified acceptable hardness and strength for H Conditions, see Table 3.2.1.8.

1.6.3 *[Figure]* Effect of aging temperature on hardness of bar.

1.6.4 *[Figure]* Effect of aging time on hardness of bar.

1.6.5 *[Figure]* Effect of aging time on hardness of bar.

1.6.6 *[Figure]* Effect of aging temperature on hardness of bar.

1.6.7 *[Figure]* Effect of holding time at the aging temperature on hardness and notch tensile strength of bar.

1.6.8 *[Figure]* Effect of aging time on hardness and notch tensile strength for specimens aged at a lower temperature subsequent to pre-aging for 2 hours at a higher temperature.

1.6.9 *[Figure]* Effect of aging time at 752F and 842F on hardness of base and weld metal.

1.7 Forms and Conditions Available

The alloy is produced in the forms of billets, plate, bar, and wire. It is usually supplied solution treated to Condition A, ready for fabrication and subsequent hardening by the user. However, it can be supplied in hardened conditions, if desired. Recommended conditions for certain fabrication processes are discussed in Section 4. (Fabrication).

1.8 Melting and Casting

1.8.1 Melting. The alloy is produced by electric arc melting in air or by consumable electrode vacuum arc or electroslag remelting. Vacuum arc remelting lowers gas content, reduces and disperses inclusions, and minimizes alloy segregation during solidification. These factors, coupled with the elimination of delta ferrite (as a result of its basic compositional difference from 17-4PH which is not delta ferrite-free), results in superior transverse mechanical properties in all locations within the product compared to 17-4PH.

1.8.2 Casting. The alloy is readily castable and is used for castings in jet engines and aircraft, processing equipment, and nuclear reactors. It is also used for cast parts in valves, controls, compressors and intricately shaped parts requiring high strength plus corrosion resistance. To meet the specified mechanical properties for 15-5PH alloy, the composition of castings should be within the limits shown in Table 1.4.2. The lower copper range for sand castings is necessary so that they can be welded without danger of underbead cracking in the presence of copper and copper compounds which precipitate during slow cooling of these generally large sections. Being usually much smaller sections which cool rapidly, investment castings can tolerate more copper without the danger of underbead cracking.

Where welding is not a factor, higher levels of copper in the range 3.0 to 5.0 percent can be used. However, such castings with copper outside the specified range will not meet property specifications. Higher copper content generaly results in higher yield strength but lower ductility castings

The composition of castings must be "in balance" to achieve maximum hardening. The alloy producer suggests that castings not be rejected on composition alone since variations in analysis may be self compensating so that balance is maintained. Hardness measurements after heat treatment are suggested as a means of determining hardening capacity.

It is suggested (Ref. 46) that castings be solution treated at 1900 to 1925F for best refinement of the cast structure. If the analysis is improperly balanced and castings are non-magnetic, or fail to harden upon aging, solution treatment at a lower temperature (1700F, 1500F, or 1400F) may correct the difficulty. The lower temperature restricts carbide solution, lowers the stability of the resulting austenite, and induces considerable transformation to martensite.

If the 1900F solution treatment is not applied to castings of recommended analysis, maximum tensile and yield strengths, ductility, and hardness may not be obtained.

A double solution treatment at 1900F is effective in refining grain size and improving ductility and impact strength.

Castings should be soaked 15 minutes to an hour at 1900 to 1925F, then air or oil cooled to 70F or lower. If reheating for the aging treatment begins before 70F has been reached, full hardening may not be achieved. After solution treatment, the alloy is age hardened in the range 925 to 1150F. For maximum strength, it is recommended that the casting be precipitation hardened at 925F for 90 minutes followed by air cooling to room temperature.

To minimize distortion in large or intricate castings, a lower solution treatment (1700) may be advisable. Slightly lower tensile and yield strengths usually result from this treatment, but may be adequate for the application.

1.8.2.1 Room temperature axial-load high-cycle fatigue strength of machined and as-cast specimens from welded and unwelded vacuum casting. (See Figure 3.5.1.8)

1.8.2.2 Room temperature tension-compression high-cycle fatigue strength of specimens machined from cast cylinders and from a lag damper casting. (See Figure 3.5.1.9)

1.8.2.3 Room temperature axial-load high-cycle fatigue strength of specimens machined from bars vacuum cast into either production or high thermal conductivity shell molds, and subsequently HIP'd or not HIP'd. (See Figure 3.5.1.10)

1.8.2.4 Room temperature axial-load high-cycle fatigue strength of HIP'd and not HIP'd notched ($K_t = 3.0$) specimens machined from shell mold castings and notched ($K_t = 3.0$) specimens machined from HIP'd lag damper casting. (See Figure 3.5.1.11)

1.9 Special Considerations

1.9.1 Directional ductility. Precipitation-hardening stainless steel alloys are used in many applications requiring large and medium size sections. In many cases, loading transverse to the fiber is involved. It has been demonstrated (Ref. 3) that certain structural characteristics, particularly delta ferrite and some precipitates, cause substantial reductions in transverse ductility, and presumably fracture toughness, for many of these alloys. For compositions in which delta ferrite is present, vacuum remelting does not improve this situation.

15-5PH is a delta ferrite-free compositional modification of 17-4PH alloy containing less chromium and slightly higher nickel. Its short-transverse ductility at edge and intermediate locations is superior to 17-4PH in heavy sections. However, in products made from air cast ingots of 15-5PH, the short-transverse ductility at the center location may be lower than at edge or intermediate locations (See Table 3.2.1.11). This nonuniformity of ductility is evidently the result of gross segregation (Ref. 3) which may be reduced by vacuum remelting (Table 3.2.1.11).

1.9.2 Embrittlement. Martensitic and precipitation-hardening stainless steels are subject to an embrittling reaction when heated in the approximate temperature range 500 to 900F. This is evidenced by an increase in yield strength and a reduction in the resistance to crack propagation. Its magnitude depends on a number of factors including the exposure time, composition, and previous treatment.

Insufficient data are available to quantitatively define the effects of these variables for any of the commercial steels subject to this embrittlement. However, on the basis of the information available for the PH steels (alloy codes 1501 through 1510), it would be expected that long time exposures at temperatures in the lower portion of the embrittling range would produce the maximum embrittling effects.

It has been reported (Refs. 11, 35) that the embrittlement is associated with the formation of a copper-rich alpha prime ferrite phase and that the following factors are important in establishing its magnitude:

1. Increased amounts of chromium, silicon and columbium increase the rate of embrittlement at 800F. When silicon and columbium are low, chromium becomes the sole controlling factor, except that the nickel content as related to the chromium influences the result (Cr-Ni balance influences the martensite reaction). The highest nickel content which can be used at a given level of chromium without inhibiting martensite transformation is best from the standpoint of embrittlement.

2. Aluminum and apparently titanium increase the rate of embrittlement at 800F.

3. The embrittlement is completely reversible by reapplying the initial precipitation-hardening temperature, if that temperature is 1025F or higher.

4. Lowering the solution-treating temperature, at least down to 1650F, slightly lessens the tendency toward embrittlement at 800F.

1.9.3 Composition limits. Consumers have sometimes complained that the composition limits of precipitation-hardenable semi-austenitic steels are too wide to permit uniform response to heat treatment (Ref. 8). The impact strength of 17-4PH type precipitation-hardening stainless steel both before and after exposure at 800F are affected by variations in chemistry within the recommended composition range (Ref. 11). It would be expected that 15-5PH would be similarly affected.

1.9.4 Solution treated material. For many applications, 15-5PH should not be used in Condition A. The structure is untempered martensite that has low ductility and poor resistance to stress corrosion cracking (See Figure 2.3.2.6).

1.9.5 Mechanical hysteresis. Force transducers made from this alloy can give erroneous indications of strain due to a nonlinear, anelastic stress-strain relationship known as mechanical hysteresis. The amount of mechanical hysteresis is mainly controlled by heat treatment. A specially developed heat treatment process can substantially reduce hysteresis error, and thus improve force transducer accuracy (Ref. 31).

1.9.5.1 *[Table]* Effect of heat treatment on shear beam force transducer mechanical hysteresis.

1.9.6 Hydrogen embrittlement. (See section 4.4.6)

2 PHYSICAL PROPERTIES AND ENVIRONMENTAL EFFECTS

2.1 Thermal Properties

2.1.1 Melting range.

2.1.2 Phase changes. This is a martensitic alloy which undergoes transformation from austenite to martensite above room temperature, upon cooling from an austenitizing temperature of about 1900F. During austenitizing (also a solution treatment), all of the copper (the precipitation-hardening agent) is dissolved in the austenite. On cooling from this treatment, martensite transformation (Ms) starts normally at about 250F and is virtually complete at 90F. After cooling, the structure consists of a "soft martensite" supersaturated with copper. During subsequent hardening treatment a copper-rich phase is precipitated in the martensite matrix and, at the same time, the matrix is stress relieved or tempered.

2.1.3 *[Figure]* Thermal conductivity.

2.1.4 *[Figure]* Thermal expansion.

2.1.5 *[Table]* Specific heat.

2.1.6 Thermal diffusivity.

2.2 Other Physical Properties

2.2.1 *[Table]* Density.

2.2.2 *[Table]* Electrical resistivity.

2.2.2.1 *[Figure]* Effect of 10-minute aging temperature on change in electrical resistivity and its temperature derivative.

2.2.2.2 *[Figure]* Effect of aging time on change in electrical resistivity over a range of aging temperatures.

2.2.2.3 *[Figure]* Effect of 2-hour aging temperature on electrical resistivity and its temperature derivative for specimens pre-aged at 1040F for 2 hours.

2.2.2.4 *[Figure]* Effect of aging time on electrical resistivity for specimens aged at various temperatures subsequent to 1040F, 2 hour pre-age.

2.2.3 Magnetic properties.

2.2.3.1 *[Figure]* Induction curves.

2.2.3.2 *[Figure]* Hysteresis curves.

2.2.4 Emittance.

2.2.5 Damping capacity.

2.3 Chemical Properties.

2.3.1 Corrosion resistance. The general level of corrosion resistance of this alloy exceeds that of Types 410 and 431 stainless steels (Ref. 27). It is comparable to Type 304 stainless steel in most media and similar to that of 17-4PH (Refs. 1, 4, 7). In boiling 65 percent $HN0_3$ and in 1 percent HCl, 15-5PH and 17-4PH exhibit about the same resistance. In salt fog and chloride pitting solutions, 15-5PH exhibits somewhat superior resistance as shown in Table 2.3.1.1.

In all heat treated conditions, 15-5PH exhibits very little rusting during 500 hours' exposure to 5-percent salt fog at 95F (Ref. 27). When exposed to seacoast atmospheres for long periods of time, it gradually develops a superficial layer of rustlike other precipitation-hardening stainless steels (Ref. 27). The general level of corrosion resistance is best in the fully hardened condition, and decreases slightly as the aging temperature is increased (Ref. 27).

2.3.1.1 *[Table]* Corrosion of consumable electrode vacuum arc remelted 15-5PH and air melted 17-4PH in several corrosive media.

2.3.2 Stress corrosion cracking. The stress corrosion cracking resistance of 15-5PH is reported to be superior to 17-4PH in boiling 42 percent $MgCl_2$ solutions but slightly inferior to 17-4PH in H_2S-NaCl-Acetic Acid solutions (Ref. 1).

The results in Table 2.3.2.1 show the alloy to be highly resistant to stress corrosion cracking in aqueous salt environments in conditions H 1000 and H 1050 in that no failures were encountered even when the material was stressed to 100 percent of F_{ty}. Failures did occur, however, in the fully hardened H 900 condition but only at very high stress; i.e., 100 percent F_{ty}. As with 17-4PH, 15-5PH has the greatest degree of resistance to stress-corrosion cracking when heat treated at the highest aging temperature (1100F being preferred) (Ref. 1).

2.3.2.1 *[Table]* Stress corrosion cracking behavior of bar in three salt media.

2.3.2.2 *[Table]* Stress corrosion cracking of strip in marine atmosphere.

2.3.2.3 *[Table]* Effect of aqueous salt environment and specimen orientation on stress corrosion cracking, K_{Iscc}.

2.3.2.4 *[Table]* Tensile, plane strain fracture toughness, and stress corrosion stress intensity factor in 3.5 percent aqueous salt solution for air melted and CVM billet in H 900 and H 1000 conditions.

2.3.2.5 GTA welded stress-corrosion specimens of 1/8 inch thick 15-5PH plate in the H 1025 and H 1100 conditions have shown no evidence of cracking in 283 days exposure at the Kure Beach, North Carolina, 80-foot lot while stressed as bent beams to 90 percent of the room temperature yield strengths (Refs. 1, 7, 12).

2.3.2.6 *[Figure]* Sulfide stress corrosion cracking of rod.

2.3.3 Oxidation resistance. The oxidation resistance of this alloy is superior to Type 410 but inferior to Type 430.

2.4 Nuclear Environments

3 MECHANICAL PROPERTIES

3.1 Specified Mechanical Properties

3.1.1 *[Table]* Producer's guaranteed mechanical properties.

3.1.2 *[Table]* AMS specified mechanical properties for air melted alloy products.

3.1.3 *[Table]* AMS specified mechanical properties for consumable electrode vacuum arc remelted alloy products.

3.1.4 *[Table]* AMS and ASTM specified strength, hardness, and bendability of solution heat treated sheet, strip, and plate.

3.1.5 *[Table]* AMS and ASTM specified tensile strength and hardness for solution heat treated bars, forgings, flash welded rings, and wire.

3.1.6 *[Table]* AMS and ASTM specified tensile properties and hardness for precipitation hardened sheet, strip, and plate.

3.1.7 *[Table]* AMS and ASTM specified tensile properties and hardness for precipitation hardened bars, forgings, flash welded rings, extrusions, and stock for forging, flash welded rings, or extruding.

3.1.8 *[Table]* AMS specified tensile properties and hardness for precipitation hardened investment castings.

3.1.9 *[Table]* AMS specified tensile properties and hardness for precipitation hardened tubular centrifugal castings.

3.1.10 *[Table]* Producer's specified acceptable tensile properties and hardness for Condition A.

3.1.11 *[Table]* Producer's specified acceptable tensile properties and hardness for sheet and strip in H Conditions.

3.2 Mechanical Properties at Room Temperature

3.2.1 Tension Stress-Strain Diagrams and Tensile Properties.

3.2.1.1 *[Table]* Typical mechanical properties for bar.

3.2.1.2 *[Table]* Typical mechanical properties for sheet and strip.

3.2.1.3 *[Table]* Effects of section size, specimen location and specimen direction on tensile properties of arc melted and vacuum remelted stock in H 900 condition.

3.2.1.4 *[Table]* Room temperature tension, compression, shear, and bearing properties of plate in H 1025 condition, for which fatigue properties appear in Figures 3.5.1.6 and 3.5.1.7.

3.2.2 Compression Stress-Strain Diagrams and Compression Properties. (See also Table 3.2.1.4)

3.2.3 Impact (see also Section 3.3.3).

3.2.4 Bending.

3.2.5 Torsion and shear. (See also Table 3.2.1.4)

3.2.5.1 *[Table]* Shear strength in torsion.

3.2.5.2 *[Table]* Shear strength in double shear for H 900 condition.

3.2.5.3 *[Figure]* Effect of aging temperature (H Condition) on shear strength in double shear.

3.2.6 Bearing. (See also Table 3.2.1.4)

3.2.6.1 *[Table]* Bearing strength of plate in H 1025 condition.

3.2.6.2 *[Table]* Bearing strength of bar in H 1150 condition.

3.2.7 Stress concentration.

3.2.7.1 Notch properties.

3.2.7.1.1 Effect of holding time at the aging temperature on hardness and notch tensile strength of bar. (See Figure 1.6.7)

3.2.7.1.2 Effect of aging time on hardness and notch tensile strength for specimens aged at a lower temperature subsequent to pre-aging for 2 hours at a higher temperature. (See Figure 1.6.8)

3.2.7.2.2 *[Figure]* Effect of aging temperature on notch tensile strength of bar.

3.2.7.2 Fracture toughness.

3.2.7.2.1 *[Figure]* Effect of age (H condition) temperature on tensile properties and plane strain fracture toughness.

3.2.7.2.2 Influence of final forge temperature on tensile properties and plane strain fracture toughness. (See Figure 4.1.1.1)

3.2.7.2.3 Tensile, plane strain fracture toughness, and stress corrosion stress intensity factor in 3.5 percent aqueous salt solution for air melted and CVM billet in H 900 and H 1000 conditions. (See Table 2.3.2.4)

3.2.7.2.4 *[Table]* J-integral fracture toughness of plate and weldment.

3.2.8 Combined Loading.

3.3 Mechanical Properties at Various Temperatures (see also Section 3.2)

3.3.1 Tension Stress-Strain Diagrams and Tensile Properties.

3.3.1.1 *[Figure]* Effect of test temperature on tensile properties of bar in H 925 condition.

3.3.1.2 *[Figure]* Effect of test temperature on tensile properties of bar in H 1025 condition.

3.3.1.3 *[Figure]* Effect of test temperature on tensile properties of bar in H 1100 condition.

3.3.1.4 *[Figure]* Effect of test temperature on tensile properties of bar in H 1150-M condition.

3.3.2 Compression Stress-Strain Diagrams and Compression Properties.

3.3.2.1 *[Figure]* Typical compressive stress-strain and tangent-modulus curves at selected temperatures for bar in H 1025 condition.

3.3.2.2 *[Figure]* Typical compressive stress-strain and tangent-modulus curves at selected temperatures for bar in H 1150 condition.

3.3.2.3 *[Figure]* Effect of test temperature on compressive yield strength of bar in H 1025 condition.

3.3.2.4 *[Figure]* Effect of test temperature on compressive yield strength of bar in H 1150 condition.

3.3.3 Impact.

3.3.3.1 *[Table]* Charpy-V impact energy for sheet at room temperature and -65F.

3.3.3.2 *[Figure]* Effect of temperature on Charpy-V impact energy for Condition H 1150-M.

3.3.4 Bending.

3.3.5 Torsion and shear.

3.3.6 Bearing.

3.3.7 Stress concentration.

3.3.7.1 Notch properties.

3.3.7.2 Fracture toughness.

3.2.7.2.1 *[Figure]* Effect of test temperature in the range -4 to +72F on the tensile properties and plane strain fracture toughness.

3.2.7.2.2 *[Table]* Effect of aged condition, test temperature, and specimen orientation on strength and plane strain fracture toughness.

3.3.8 Combined properties.

3.4 Creep and Creep Rupture Properties

3.4.1 *[Figure]* Creep deformation and rupture curves at selected temperatures for forged bar in H 1025 condition.

3.5 Fatigue Properties

3.5.1 Conventional high-cycle fatigue.

3.5.1.1 *[Figure]* Room temperature axial-load fatigue strength of CVM billet in H 925 and H 1075 conditions.

3.5.1.2 *[Figure]* Room temperature longitudinal unnotched axial-load constant-life fatigue diagram for bar.

3.5.1.3 *[Figure]* Room temperature transverse unnotched axial-load constant-life fatigue diagram for bar.

3.5.1.4 *[Figure]* Room temperature londitudinal and transverse notched (K_t = 3.0) axial-load constant-life fatigue diagram for bar.

3.5.1.5 *[Figure]* Mild-notch axial-load fatigue strength of bar in H 1025 condition at stress ratios, R = 0.5, 0.1, -1.0.

3.5.1.6 *[Figure]* Room temperature axial-load fatigue strength of plate in H 1025 condition.

3.5.1.7 *[Figure]* Room temperature axial-load notched (K_t = 3.0) fatigue strength of plate in H 1025 condition.

3.5.1.8 *[Figure]* Room temperature axial-load high-cycle fatigue strength of machined and as-cast specimens from welded and unwelded vacuum castings.

3.5.1.9 *[Figure]* Room temperature tension-compression high-cycle fatigue strength of specimens machined from cast cylinders and from a lag damper casting.

3.5.1.10 *[Figure]* Room temperature axial-load high-cycle fatigue strength of specimens machined from bars vacuum cast into either production or high thermal conductivity shell molds, and subsequently HIP'd or not HIP'd.

3.5.1.11 *[Figure]* Room temperature axial-load high-cycle fatigue strength of HIP'd and not HIP'd notched (K_t = 3.0) specimens machined from shell mold castings and notched (K_t = 3.0) specimens machined from HIP'd lag damper casting.

3.5.1.12 *[Figure]* Elevated temperature transverse unnotched axial-load fatigue strength of forged bar.

3.5.1.13 *[Figure]* Elevated temperature transverse notched (K_t = 3.0) axial-load fatigue strength of forged bar.

3.5.2 Low-cycle Fatigue

3.5.3 Fatigue Crack Propagation.

3.5.3.1 *[Figure]* Room temperature fatigue crack growth rate at 10 Hz, R = 0.05 for plate in H 1050 condition.

3.5.3.2 *[Figure]* Room temperature fatigue crack growth rate at R = 0.67, trapezoidal load wave form (1-minute hold times), for plate in H 1050 condition.

3.5.3.3 *[Figure]* Room temperature fatigue crack growth rate at 10 Hz, R = 0.05 for plate in H 1100 condition.

3.5.3.4 *[Figure]* Room temperature fatigue crack growth rate at R = 0.05, trapezoidal load wave form (1-minute hold times), for plate in H 1100 condition.

3.5.3.5 *[Figure]* Room temperature fatigue crack growth rate in 3.5-percent NaCl solution at R = 0.05, trapezoidal load wave form (1-minute hold times), for plate in H 1100 condition.

3.5.3.6 *[Figure]* Room temperature fatigue crack growth rate at R = 0.67, trapezoidal load wave form (1-minute hold times), for plate in H 1100 condition.

3.5.3.7 *[Figure]* Room temperature fatigue crack growth rate in 3.5-percent NaCl solution at R = 0.67, trapezoidal load wave form (1-minute hold times), for plate in H 1100 condition.

3.5.3.8 *[Figure]* Effects of load ratio (R) and environment (air versus salt water) on room temperature fatigue crack growth rate for plate in H 1100 condition.

3.5.3.9 *[Figure]* Effects of load wave form (sinusoidal versus trapezoidal), load ratio (R), and heat treated condition (H) on room temperature fatigue crack growth rate for plate.

3.5.3.10 *[Figure]* Fatigue crack growth rate in air and 3.5 percent aqueous NaCl solution for the H 1025 and H 1100 conditions.

3.6 Elastic Properties

3.6.1 Poisson's Ratio, 0.272 in all hardened conditions (Ref. 27).

3.6.2 Modulus of Elasticity.

3.6.2.1 *[Table]* Elastic moduli in tension and in torsion.

3.6.2.2 *[Figure]* Effect of temperature on modulus of elasticity.

3.6.2.3 *[Figure]* Effect of temperature on modulus of elasticity in compression of bar in H 1025 condition.

3.6.2.4 *[Figure]* Effect of temperature on modulus of elasticity in compression of bar in H 1150 condition.

3.6.3 Modulus of Rigidity.

3.6.4 Tangent Modulus.

3.6.5 Secant Modulus.

4 FABRICATION

4.1 Forming

4.1.1 Forging. Elimination of delta ferrite gives this alloy improved forging properties over 17-4PH in critical upset forgings and hot flattening operations (Refs. 1, 2, 4). Materials for forging should be ordered "overaged for forging," a condition which also allows cold sawing of large sections without cracking (Ref. 1).

Forging blanks less than 3/4 inch diameter or thickness should be heated uniformly to 2150 to 2200F and held at temperature at least 15 minutes before forging. For sections over 3/4 inch, material should be heated 1/2 hour per inch of thickness at 2150 to 2200F and held one hour at temperature prior to forging. Heating above 2200F may cause undesirable grain coarsening.

Temperature during forging should not be allowed to drop below 1850F (Ref. 1).

After forging, material should be cooled below 90F to assure complete transformation to martensite. For better toughness in hardened condition, forged parts must first be treated to Condition A (Ref. 1).

4.1.1.1 *[Figure]* Influence of final forge temperature on tensile properties and plane strain fracture toughness.

4.1.2 Cold-forming. Forming should be limited to mild operations for Condition A. Fabrication is greatly improved by heat treating (Ref. 27). If severe cold forming is required, use Conditions H 1150 and H 1150-M (Ref. 1).

4.1.3 Cold-heading. Wire for cold heading should be ordered overaged, copper coated and cold drawn.

4.1.4 *[Table]* Minimum room temperature bend radii.

4.1.5 Primary and secondary fabrication methods, including equipment and tooling, are discussed in detail in Reference 50. Primary fabrication includes rolling, extruding, forging, and drawing of tube, rod, and wire. Secondary fabrication produces finished or semifinished parts from sheet, bar, or tube using additional metalforming operations. Secondary forming processes include brake bending, deep drawing, spinning and shear forming, drop hammer, trapped rubber, stretch, roll forming, dimpling, joggling, and sizing.

4.2 Machining and Grinding

4.2.1 The alloy can be machined in any heat treated condition. Parts machined in Condition A may be subsequently hardened with no harmful scaling or distortion. Design allowances can be made for the predictable contraction on hardening (Ref. 1). Machining rates for the alloy in Condition A are

similar to those for Type 302 or Type 304 (Ref. 1). The relative machinability of Condition H 1150-M is comparable to Type 303 (Ref. 4). Condition H 900 material should be machined at 60 percent of the rate used for Condition A.

4.3 Joining

4.3.1 Welding procedures are similar to those for austenitic stainless steel, even though the composition and structure of this alloy more closely resemble those of a martensitic type. Any arc or resistance welding process for regular grades of stainless are applicable (Refs. 1, 2). The usual weld filler employed is AWS A5.9 Classification ER 630. Resolution annealing is unnecessary (Ref. 7).

Autogenous welding (no filler) methods such as LW and EBW should be used with caution since the lack of ferrite forming potential can lead to hot cracking if stresses are sufficiently high. Autogenous CO_2 laser beam welds between 15-5PH and HP 9-4-20 exhibited hot-cracking, attributed to the formation of a NbC-austenite eutectic constituent (Ref. 34).

Although the alloy can be welded in any condition, the overaged conditions are preferred for highly constrained joints. If welded in condition A, or in the condition of use, or in a lower temperature aged condition than that intended for component use, then a simple post-weld aging at the desired H condition will impart weld properties comparable to those of the base metal, but possibly with somewhat less ductility and toughness. If the material is overaged (e.g. H 1150) for welding and a high final strength is desired (e.g. H 900 condition), then subsequent to welding, the component must be re-solution treated prior to aging. Otherwise, as-welded strength will be similar to that of the H 1150 condition.

The alloy's low carbon content restricts the hardness of rapidly cooled material and avoids the formation of cracks in the weld metal and heat-affected zone. This eliminates the need for preheating (Refs. 1, 2). While the alloy shows no susceptibility to spontaneous underbead cracking from weld hardening, it does not possess the high ductility and toughness of austenitic Cr-Ni steels. Therefore it should not be subjected to high levels of biaxial or triaxial stress from severely restrained weldments or exposed to notched conditions (Ref. 1).

With W-17-4PH electrodes and welding rods [specifications AMS 5827D (Ref. 22) and AMS 5825EA (Ref. 20) respectively], or 15-5PH welding wire [specification AMS 5826B (Ref. 21)], mechanical properties of the weld are equivalent to those of the base metal. Likewise , where weld deposits need to have the strength of the base metal, an E308 stainless steel electrode may be used (Ref. 2). For selected applications, the use of ER308L filler metal for the first and second passes and a 17-4PH or PH13-8Mo filler for subsequent passes has proven successful. Types 309 or 309-Cb electrodes are recommended for joining 15-5PH with dissimilar metals.

State-of-the-art welding of precipitation-hardening stainless steels is reviewed in Reference 30. Welding preparation, specific welding processes, and joint quality are exhaustively discussed. A systematic study of weld filler metal compositions, with the goal of developing a weld chemistry for the 15-5PH/17-4PH alloy system joint that would exhibit comparable properties regardless of whether it was solution treated and aged or aged only after welding, is described in Reference 43. General guidelines for weld wire composition are presented, but no specific composition is recommended.

4.3.2 *[Table]* Weld electrode and wire compositions.

4.4 Surface Treating

4.4.1 Air is a satisfactory furnace atmosphere for heat treating this alloy. Fuel-fired furnaces, where c ombustion products might contaminate the work-piece surfaces, should be avoided (Ref. 7).

4.4.2 Hardening treatments produce only a light heat tint on surfaces. It is easily removed by pickling 3 to 5 minutes in 10 percent nitric-2 percent hydrofluoric acid (by volume) at 110 to 140F. This treatment also passivates or cleans the surfaces for maximum corrosion resistance. Where pickling is undesirable, heat tint may be removed by electropolishing (Refs. 1, 2, 7).

4.4.3 A two-step procedure will remove scale formed by forging or solution treating. First, the part is immersed in caustic permanganate at 160 to 18OF for one hour. After a water rinse, it is pickled in the HNO_3-HF solution used for removing tint. A hot water rinse, high pressure water or a brush scrubbing completes descaling.

4.4.4 Nitriding. There are three methods for nitrogen penetration into the alloy, corresponding to three energy levels of implantation: (1) low energy liquid and gas nitriding; (2) medium energy ion nitriding; (3) high energy ion implantation. The first method is widely used; the second and third are newer and therefore less widely used.

The results of a study (Ref. 47) of nitriding parameters on "white" and "diffusion" layers are presented in Figures 4.4.4.1 through 4.4.4.5. Nitriding temperature, time, gas pressure and flow rate were systematically varied. Composition of the gas mixture [40 vol.%N_2, 40 vol. % Ar, and 20 vol. % H_2] and the distance between cathode and anode were held constant. The study concluded the optimum conditions for ion nitriding aged 15-5PH to be one hour at 840F at gas pressure of 8 Torr and flow rate of 2.93 in^3/min. Under these conditions a "diffusion " layer free of a

"white" layer is produced. It is possible to select other parameters to produce a thicker "diffusion" layer, while the thickness of the "white" layer remains below specified limits (Ref. 47).

4.4.4.1 *[Figure]* Effect of nitriding treatment time on "white" layer thickness.

4.4.4.2 *[Figure]* Effect of nitriding treatment time and temperature on "diffusion" layer thickness.

4.4.4.3 *[Figure]* Effect of nitriding reactor pressure on "white" and "diffusion" layer thicknesses.

4.4.4.4 *Figure]* Effect of nitriding treatment temperature on thicknesses of "white" and "diffusion" layers.

4.4.4.5 *[Figure]* Effect of nitriding gas flow rate on "white" and "diffusion" layer thicknesses.

4.4.4.6 A nitrided surface adds resistance to galling and wear. The gas-phase method of nitriding produces case hardnesses of approximately R_c 67 to a depth of 0.004 to 0.006 inch. It employs a temperature of about 1050F and produces a tough core with a hardness of about R_c 36. Nitriding slightly decreases the corrosion resistance of this alloy as it does with any stainless steel (Ref. 2).

4.4.4.7 Nitriding by the proprietary Malcomizing process raises the smooth fatigue endurance limit for the H 1100 condition in reversed bending by 15 percent.

4.4.4.8 *[Figure]* Effect of nitriding (proprietary Malcomizing) on smooth and mild notch rotating beam fatigue strength of bar in H 1100 condition.

4.4.4.9 Ion nitriding (also called glow discharge or plasma nitriding), relatively new, has the advantages of short heat treatment time, low treatment temperature, minimal product distortion, cleanliness and low energy consumption. It is especially well suited to this alloy in that removal of oxide layer is unnecessary and the aging and nitriding treatments can be combined into a single-step operation. An additional advantage is that the thicknes of the diffusion zone and the "white" layer and their microstructure and composition can be controlled by the nitriding treatment parameters: composition, pressure, and flow rate of the gas as well as the temperature, voltage, and current.

4.4.5 Friction and wear of 15-5PH are reduced substantially by ion implantation of Ti and C. Results (Ref. 36) for polished samples implanted to fluences of $5x10^{14}$ Ti/mm^2 at 180, 150, 120, and 90 keV, in that order, and $2x10^{15}$ C/mm^2 at 30 keV are shown in Figures 4.4.5.1 and 4.4.5.2. Ti concentration based on previous work in Fe were estimated to range from approximately 20 atomic percent over a depth of 2 μ-in., to approximately 10 atomic percent at 3 μ-in., and to zero at approximately 6 μ-in. C concentration profiles were estimated to be nearly identical to Ti concentration profiles.

The friction coefficient (Figure 4.4.5.1) is reduced about 50 percent by ion implantation for all loads studied, seemingly independent of pin material, and due to the production of an amorphous surface layer by the implanted ions (Ref. 37). For all tests in Figure 4.4.5.1, the coefficient of friction initiated at a value between 0.2 to 0.7 gradually increased 20 to 100 percent over 100 to 250 cycles, and then remained essentially constant over the balance of 1000 cycles. Only the final coefficient of friction after 1000 cycles is shown in Figure 4.4.5.1.

Maximum wear depth results after 1000 cycles of unlubricated wear are shown in Figure 4.4.5.2. Wear increased with load at rates somewhat independent of pin material. At the lowest loads, the mean maximum wear depth ($\overline{MWD}$) was decreased by ion implantation to 5 percent of the value of the unimplanted samples. For the 440C pins, this beneficial reduction in wear completely disappeared at loads > 30 g, whereas for the 304 pins a reduced wear depth corresponding to 66 percent of the unimplanted value persisted to the highest load studied (50 g).

Wear scar diameter on the harder 440C pins was less than 0.001 in for both ion implanted and unimplanted plates at all Hertzian stress levels. Wear scar diameters on the softer 304 pins varied with stress and plate condition (See Table 4.4.5.3), and were significantly less when mating was with an ion implanted plate. The 304 pins were shortened by wear a maximum of 0.001-in when mated with unimplanted plates and by a maximum of 0.0002-in when mated with implanted plates.

Wear tracks topography was characterized by fine parallel grooves at low Hertzian stress levels, changing to galling and debris generation which increased with increasing stress at the higher stress levels. The change in wear track topography occured at the stress level where reduction in wear due to implantation disappeared.

Implanted plates had no titanium in the wear tracks after 1000 cycles at stresses > 146 ksi, but significant amounts remained at lesser stresses. Wear scars on the pins evidenced transfer films containing titanium, in larger amounts for the 304 pins than for the 440C pins.

The above study was repeated (Ref. 38) using N^+ ion implantation as the variable affecting dry friction and wear behavior. Polished samples were implanted to fluences of $4.0x10^{17}$ N^+/cm^2 at 50keV. Peak concentration was 45 atomic percent at a depth of 2.8 μ-in. dropping to about 10 atomic percent at 4.7 μ-in. The implanted alloy exhibited reduced wear at low Hertzian stresses but no significant reduction in the friction coefficient (Figures 4.4.5.5 and 4.4.5.4, respectively). At the lowest normal load studied

(12.3g = 123 ksi Hertzian stress), the average maximum wear depth of the N^+ implanted alloy (about 0.04 μ-in.) was only about 10 percent of the unimplanted value; but at normal loads of 50g (236 ksi) or above, the benefit of implantation disappears (see Figure 4.4.5.5). With the exception of 304 pin wear, implantation with Ti and C ions reduced friction and wear twice as effectively as N^+ ion implantation (see Figure 4.4.5.6).

4.4.5.1 *[Figure]* Influence of titanium and carbon ion implantation on unlubricated friction coefficient after 1000 pin-on-disc revolutions.

4.4.5.2 *[Figure]* Influence of titanium and carbon ion implantation on unlubricated wear depth after 1000 pin-on-disc revolutions.

4.4.5.3 *[Table]* 304 stainless steel pin wear in pin-on-disc tests of Ti and C ion implanted plates and of unimplanted plates.

4.4.5.4 *[Figure]* Influence of N^+ implantation on unlubricated friction coefficient after 1000 pin-on-disc revolutions.

4.4.5.5 *[Figure]* Influence of N^+ implantation on unlubricated wear depth after 1000 pin-on-disc revolutions.

4.4.5.6 *[Figure]* Influence of ion implantation (Ti and C or N^+) on unlubricated friction coefficient and mean maximum wear depth at 173 ksi Hertzian stress, expressed as ratios of unimplanted to implanted values.

4.4.6 One of the chief drawbacks of PH stainles steels is their susceptibility to hydrogen embrittlement. General sensitivity to hydrogen embrittlement is demonstrated in Figure 4.4.6.1, where the ductility of electrochemically charged and uncharged tension specimens is compared over a broad range of tensile strength for a typical PH stainless steel. Ductility loss for 15-5PH alloy in two aged conditions, cathodically charged by immersion in a 10 percent H_2SO_4 solution containing 10 mg/l of AS_2O_3 as a poison, at a current density of 90 A/m^2 for times ranging from 0.5 to 24 hours, is shown in Figure 4.4.6.2 for time up to 8 hours. Yield strengths of charged and uncharged specimens were nearly the same. The higher strength H 1025 condition shows a significantly greater susceptibility to hydrogen embrittlement than does the H 1050 treatment. Only 8 hours of charging time is required for complete loss of ductility compared to 16 hours for the H 1050 condition (not shown). The hydrogen embrittlement appears somewhat reversible. One specimen in the H 1050 condition was charged for 8 hours and then allowed to stand at ambient room temperature for 63 hours. The subsequent tensile test showed that the ductility recovered to a significant extent, being 36 percent RA compared to 4 percent for an 8-hour charge.

Via strong binding energy to the alloy, certain additives (inhibitors) to liquid or gasious media can occupy atom sites on the alloy's surfaces, thus preventing a metal-hydrogen bond and thereby inhibiting the entry of hydrogen. These inhibiting films imposed on the surface offer protection through alteration of surface adsorption characteristics, as described in Reference 33.

In a review of the literature (Ref. 33), borax nitrite is claimed to be the most effective amongst a large number of candidate inhibitors, including phosphates, chromates, nitrates, amines, and alcohols. The effectiveness of the borax-nitrite inhibitor system was observed in both sustained-load and cyclic-load experiments.

Metallic and nonmetallic thin surface films prevent (or at least reduce) hydrogen entry if the film has a lesser binding energy for hydrogen than for the alloy, and a low hydrogen solubility and/or diffusivity. "Thin" in the context used here means coatings from a monolayer of atoms to something on the order of 10^{-6} micrometers (4×10^{-5} μ-in) in thickness; not paint, spray, or clad coatings and the like where entry of hydrogen is prevented essentially by mechanical screening barriers. "Thin" films retard hydrogen entry either through a surface adsorption effect or by possessing a low diffusivity and/or a low solubility for hydrogen. The literature review cited above (Ref. 33) offers several candidate metallic and nonmetallic surface coatings. Tungsten has the lowest hydrogen permeability of the metals studied, while TiO_2 and Al_2O_3 nonmetallic coatings are protective in thin layers of the order of 2 μ-in. TiO_2 film protection is demonstrated in Figure 4.4.6.3. Reduction in area is plotted against coating thickness for specimens hydrogen charged for four hours. The reduction in area for uncoated and uncharged specimens averaged 69 percent. That for 2 μ-in thick coated specimens was approximately 60 percent; that for 20 μ-in thick casting about 67 percent. Both casting thicknesses were effective in preventing hydrogen embrittlement.

The influence of hydrogen charging time on ductility for 20 μ-in thick TiO_2 coated specimens is shown in Figure 4.4.6.4. There is some loss in ductility for 40-hour charged specimens, but those specimens are still considerably more ductile that 4-hour charged uncoated specimens (for which the reduction in area is about 15 percent; see Figure 4.4.6.3). The literature (Ref. 33) suggests that nonmetallic films appear to be superior to metallic thin films for preventing hydrogen entry and subsequent embrittlement.

For stainless steels it is possible to thermally grow adherent oxide films of hundreds of nanometers thickness at temperatures in the vicinity of 1800F.

These films offer extensive protection and appear to be abrasion proof.

4.4.6.1 *[Figure]* Effect of strength on ductility loss for typical PH steel specimens hydrogen charged at $90A/m^2$ and tensile tested at room temperature.

4.4.6.2 *[Figure]* Effect of hydrogen charging on ductility of rod in H 1025 and H 1050 conditions.

4.4.6.3 *[Figure]* Effect of TiO_2 film thickness on ductility of specimens hydrogen charged four hours at $90A/m^2$ and tensile tested at room temperature.

4.4.6.4 *[Figure]* Effect of hydrogen charging time on ductility of TiO_2 coated (20 m-in. thick) specimens (H 1025 condition) tensile tested at room temperature after charging.

Table 1.3.1 AMS specifications for wrought products (Refs. 5, 6, 19)

Alloy	15-5PH	
Alloy Grade	Multiple Melted Using Consumable Electrode Practice During Remelting or Using Electroslag Process in the Final Melting Cycle	
Condition	A and H 900 through H 1150	
Form	Bars, Wire, Forgings, Flash Welded Rings, Extrusions, and Stock for Forging, Flash Welded Rings or Extrusions	Sheet, Strip, and Plate
AMS (Reference)	5658C (5) 5659H (6)	5862D (19)

Table 1.3.2 ASTM specifications for wrought products (Refs. 23-25)

Alloy	15-5PH		
Condition	A and H 900 through H 1150		
Form	Plate, Sheet, and Strip	Hot-rolled and Cold-finished Bars and Shapes	Forgings
ASTM Specification [Reference]	A 693-93 (XM-12) [23]	A 564/A 564M-5 (XM-12) [24]	A 705/A 705M-95 (XM-12) [25]

Table 1.3.3 AMS specifications for investment castings (Refs. 13-17)

Alloy	15-5PH
Form	Investment Castings
AMS Specification (Reference)	Condition
5346A (13)	H 925 (F_{tu} = 180 ksi)
5400 (17)	H 935 (F_{tu} = 170 ksi)
5347 (14)	H 1000 (F_{tu} = 150 ksi)
5356 (15)	H 1100 (F_{tu} = 130 ksi)
5357 (16)	A (Hardness R_C 31 max)

Table 1.3.4 AMS specifications for tubular centrifugal castings (Ref. 18)

Alloy	15-5PH
Form	Tubular Centrifugal Castings
Condition	A (Hardness BHN 363 max)
AMS Specification	5348A

Table 1.4.1 Specified composition for wrought products (Refs. 1, 5, 6, 19, 23-25, 27)

Alloy	15-5PH					
Source	Armco (1, 27) ASTM (23-25)		AMS (19)		AMS (5, 6)	
Form	All Wrought Products		Sheet, Strip, and Plate		Bars, Wire, Forgings, Flash Welded Rings, Extrusions, and Stock for Forging, Flash Welded Rings or Extruding	
Grade	Air melt or consumable electrode vacuum arc remelt		Multiple melted using vacuum-arc consumable electrode or electroslag processes in the final melt		Multiple melted using vacuum arc consumable electrode practice during remelting or electroslag process in the final melting cycle	
	Weight Percent					
	Minimum	Maximum	Minimum	Maximum	Minimum	Maximum
Carbon	—	0.07	—	0.07	—	0.07
Manganese	—	1.00	—	1.00	—	1.00
Silicon	—	1.00	—	1.00	—	1.00
Phosphorous	—	0.040	—	0.030	—	0.030
Sulfur	—	0.030	—	0.015	—	0.015
Chromium	14.00	15.50	14.00	15.50	14.00	15.50
Nickel	3.50	5.50	3.50	5.50	3.50	5.50
Copper	2.50	4.50	2.50	4.50	2.50	4.50
Columbium + Tantalum	0.15	0.45	5xC	0.45	—	—
Columbium	—	—	—	—	5xC	0.45
Tantalum	—	—	—	—	—	0.05
Molybdenum	—	—	—	0.50	—	0.50
Iron	Balance		Balance		Balance	

Table 1.4.2 Producer's specified composition for castings (Ref. 9)

Alloy	15-5PH			
Form	Castings			
Type of Casting	Investment		Sand and Centrifugal	
	Weight Percent			
	Minimum	Maximum	Minimum	Maximum
Carbon	—	0.05	—	0.05
Manganese	—	0.60	—	0.60
Phosphorous	—	0.03	—	0.03
Sulfur	—	0.03	—	0.03
Silicon	0.50	1.00	0.50	1.00
Chromium	14.5	15.5	14.5	15.5
Nickel	4.2	5.0	4.2	5.0
Copper	2.8	3.5	2.5	3.2
Columbium + Tantalum	0.15	0.30	0.15	0.30
Nitrogen	—	0.05	—	0.05
Iron	Balance		Balance	

Table 1.4.3 AMS specified composition for investment castings (Refs. 13-17)

Alloy	15-5PH			
Source	AMS (13)		AMS (14-17)	
Form	Investment Castings			
Condition/ Grade	H 925 / F_{tu} = 180 ksi		H 935 / F_{tu} = 170 ksi H 1000 / F_{tu} = 150 ksi H 1100 / F_{tu} = 130 ksi and A / Hardness = R_C 31 max	
	Weight Percent			
	Minimum	Maximum	Minimum	Maximum
Carbon	—	0.05	—	0.05
Manganese	—	0.60	—	0.60
Silicon	0.50	1.00	0.50	1.00
Sulfur	—	0.025	—	0.025
Phosphorous	—	0.025	—	0.025
Chromium	14.00	15.50	14.00	15.50
Nickel	4.20	5.00	4.20	5.50
Copper	2.50	3.20	2.50	3.20
Columbium + Tantalum	0.15	0.30	0.15	0.30
Tantalum	—	0.10	—	—
Nitrogen	—	0.05	—	0.05
Iron	Balance		Balance	

Table 1.4.4 AMS specified composition for tubular centrifugal castings (Ref. 18)

Alloy	15-5PH	
Form	Tubular Centrigugal Castings	
Condition/Grade	H 925 / F_{tu} = 180 ksi	
	Weight Percent	
	Minimum	Maximum
Carbon	—	0.05
Manganese	—	0.60
Silicon	0.50	1.00
Phosphorous	—	0.025
Sulfur	—	0.025
Chromium	14.00	15.50
Nickel	4.20	5.00
Copper	2.50	3.20
Columbium + Tantalum	0.15	0.30
Aluminum	—	0.05
Tin	—	0.02
Nitrogen	—	0.05
Iron	Balance	

Table 1.4.5 AMS specified compostition for weld electrodes and wire (Refs. 20-22)

Alloy	17-4PH		15-5PH		17-4PH	
Source	AMS (20)		AMS (21)		AMS (22)	
Form	Weld Wire		Weld Wire		Weld Electrode	
	Weight Percent					
	Minimum	Maximum	Minimum	Maximum	Minimum	Maximum
Carbon	—	0.05	0.025	0.050	—	0.05
Manganese	0.25	0.75	0.25	0.75	0.25	0.75
Silicon	—	0.75	—	0.60	—	0.75
Phosphorous	—	0.025	—	0.020	—	0.04
Sulfur	—	0.025	—	0.010	—	0.03
Chromium	16.00	16.75	14.40	15.30	16.00	16.75
Nickel	4.50	5.00	4.75	5.50	4.50	5.00
Columbium	0.15	0.30	5xC	0.40	0.15	0.30
Copper	3.25	4.00	3.00	3.50	3.25	4.00
Molybdenum	—	0.75	—	0.30	—	0.75
Tantalum	—	—	—	0.05	—	—
Aluminum	—	—	—	0.025	—	—
Oxygen	—	—	—	0.01	—	—
Nitrogen	—	—	—	0.040	—	—
Hydrogen	—	—	—	0.0006	—	—
Iron	Balance		Balance		Balance	

Table 1.5.2 Age condition A to H Conditions
(Precipitation hardening heat treatment schedules)
(Refs. 1, 2, 5, 6, 27)

Alloy	15-5PH		
Condition	Age		
	Temperature ± 15F[a]	Time (hr)	Cool
H 900	900	1	Air
H 925	925	4	Air
H 1025	1025	4	Air
H 1075	1075	4	Air
H 1100	1100	4	Air
H 1150	1150	4	Air
H 1150 + H 1150	1150 1150	4 followed by 4	Air Air
H 1150-M	1400 1150	2 followed by 4	Air Air

[a] AMS (5, 6): Temperature ± 10F, Time ± 0.3 hour.

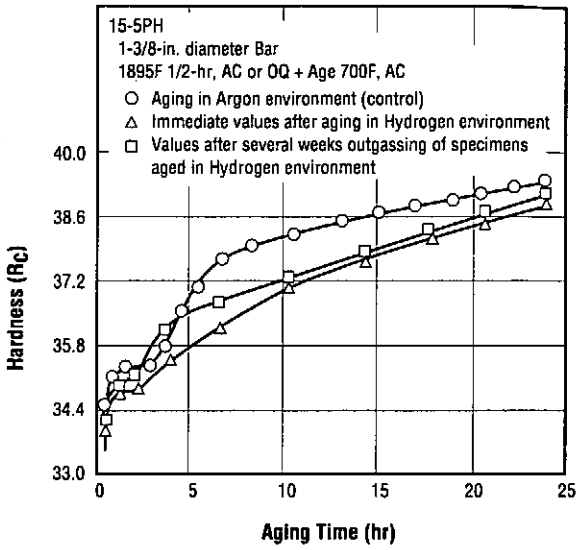

Figure 1.5.2.2.1 Influence of hydrogen aging treatment environment on age hardening at 700F (Ref. 59)

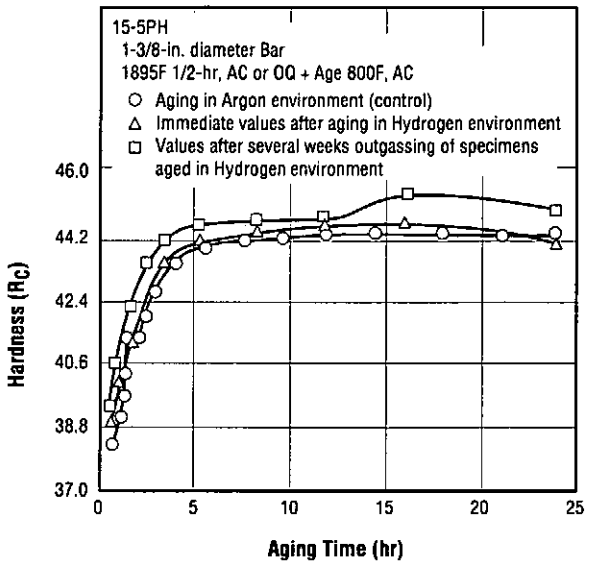

Figure 1.5.2.2.2 Influence of hydrogen aging treatment environment on age hardening at 800F (Ref. 59)

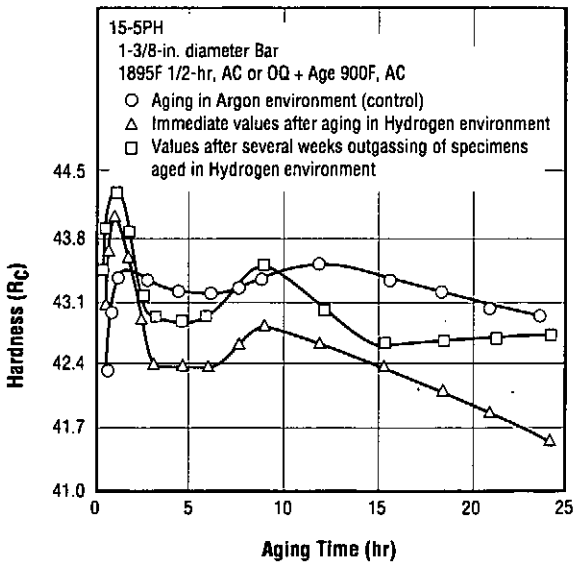

Figure 1.5.2.2.3 Influence of hydrogen aging treatment environment on age hardening at 900F (Ref. 59)

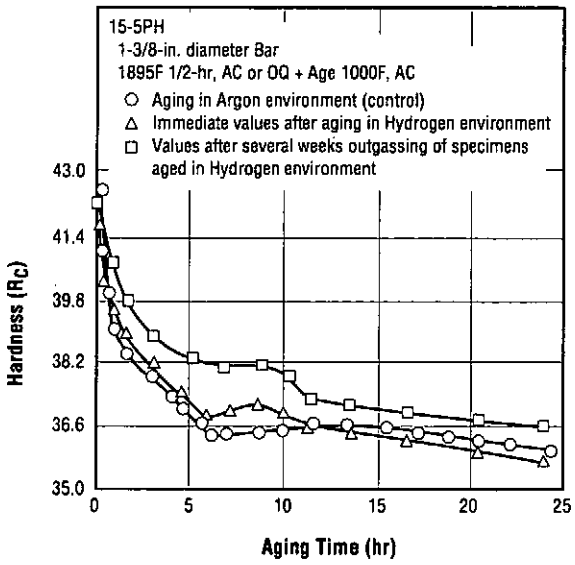

Figure 1.5.2.2.4 Influence of hydrogen aging treatment environment on age hardening at 1000F (Ref. 59)

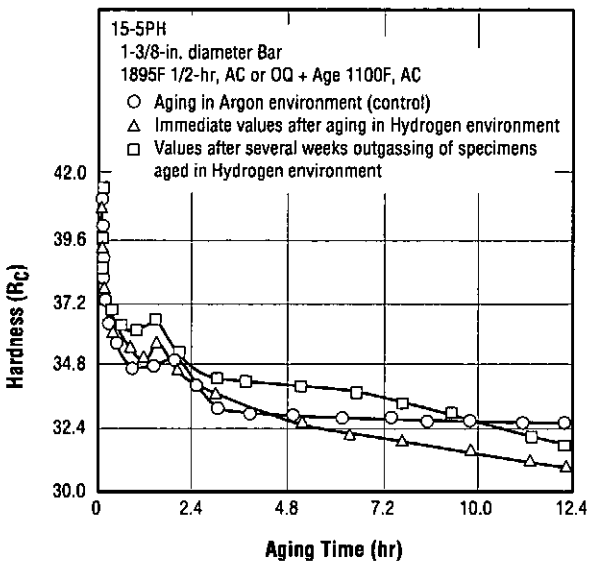

Figure 1.5.2.2.5 Influence of hydrogen aging treatment environment on age hardening at 1100F (Ref. 59)

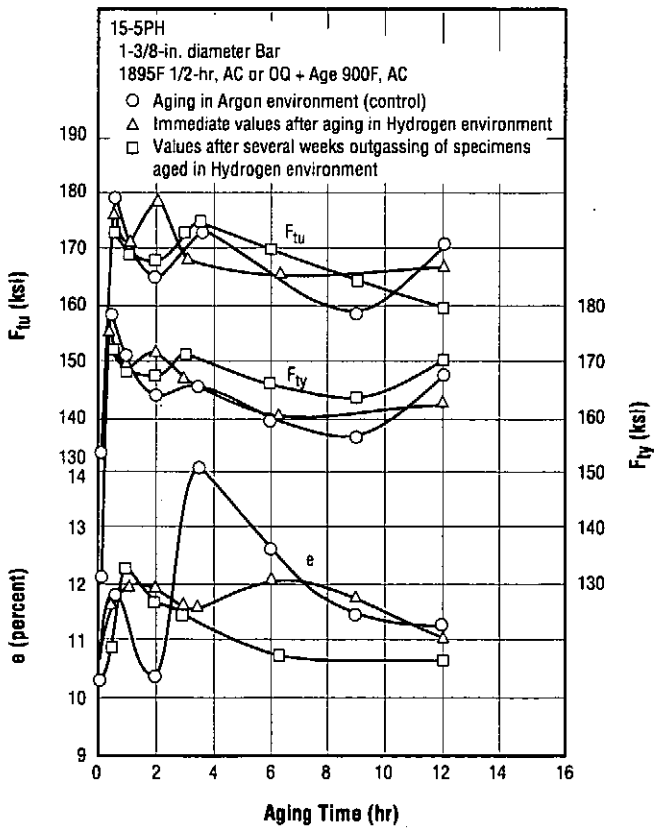

Figure 1.5.2.2.6 Influence of hydrogen aging treatment environment on 900F aged tensile properties (Ref. 59)

Table 1.5.2.3.1 Dimensional change (contraction) from hardening heat treatment (Ref. 27)

Alloy	15-5PH
Form	Sheet and Strip
Condition	Dimensional Contraction (in./in.)
H 900	0.00045
H 925	0.00051
H 1025	0.00053
H 1100	0.0009
H 1150	0.0022
H 1150M 1400 =	0.00037
1150 =	0.00206
therefore, 1400 + 1150 =	0.00243

Each value single test from single heat; can vary from heat to heat.

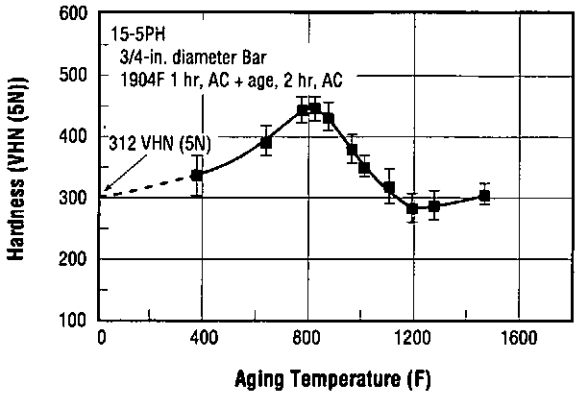

Figure 1.6.3 Effect of aging temperature on hardness of bar (Ref. 54)

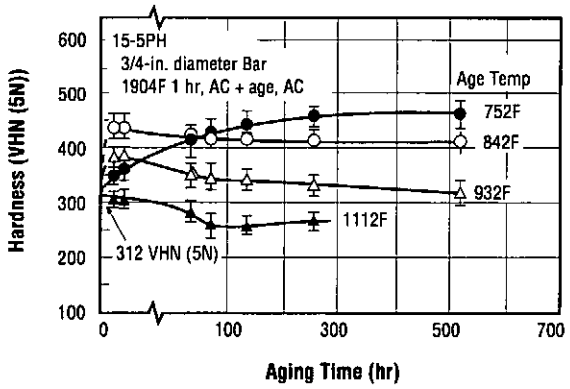

Figure 1.6.4 Effect of aging time on hardness of bar (Ref. 54)

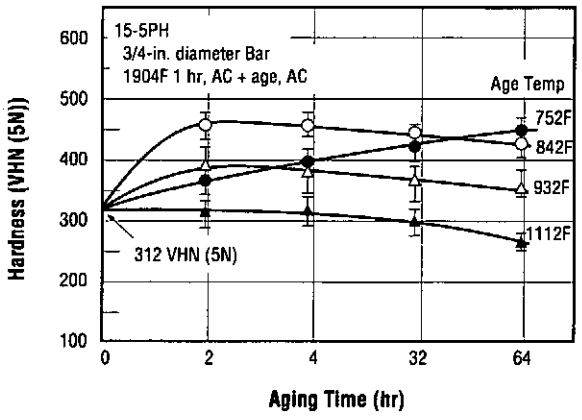

Figure 1.6.5 Effect of aging time on hardness of bar (Ref. 53)

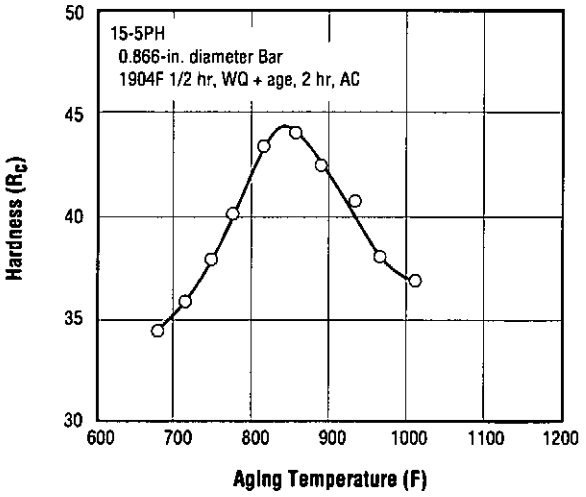

Figure 1.6.6 Effect of aging temperature on hardness of bar (Ref. 53)

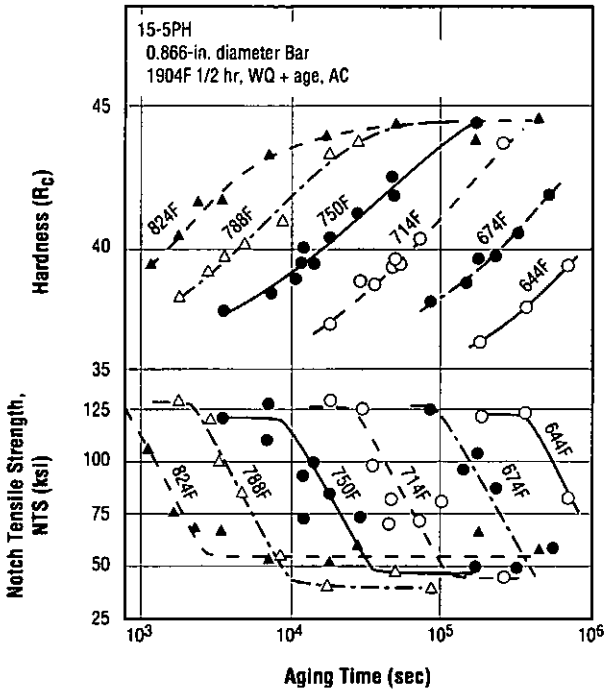

Figure 1.6.7 Effect of holding time at the aging temperature on hardness and notch tensile strength of bar (Ref. 53)

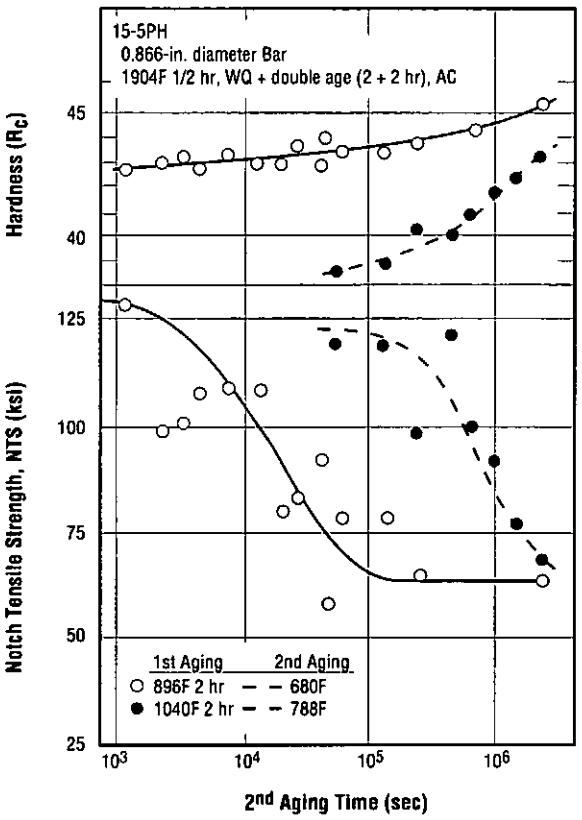

Figure 1.6.8 Effect of aging time on hardness and notch tensile strength for specimens aged at a lower temperature subsequent to pre-aging for 2 hours at a higher temperature (Ref. 53)

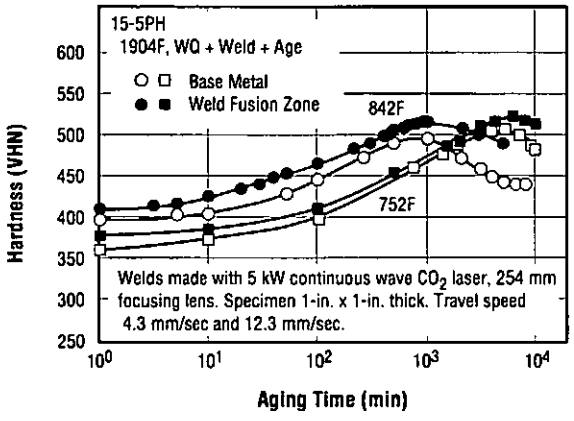

Figure 1.6.9 Effect of aging time at 752F and 842F on hardness of base and weld metal (Ref. 58)

Table 1.9.5.1 Effect of heat treatment on shear beam force transducer mechanical hysteresis (Ref. 31)

Alloy	15-5PH
Heat Treatment (Condition)	Hysteresis (μV)
H 900	7.0
Special Temperature Profile[a]	2.5
Special Temperature Profile above, but Higher Cooling Rate	2.6

[a] Proprietary; however, it is suspected that solution temperature plays a significant role and should not be too high if good hysteresis performance is to be achieved.

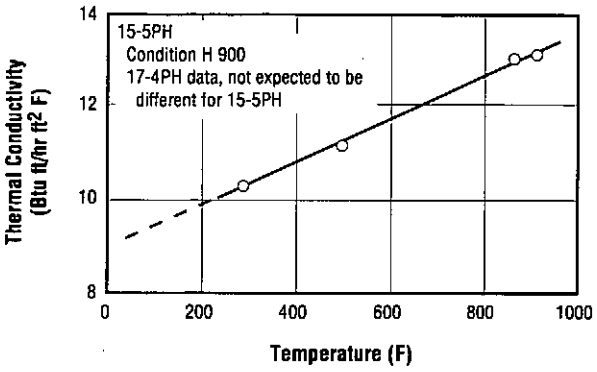

Figure 2.1.3 Thermal conductivity (Refs. 1, 7, 27)

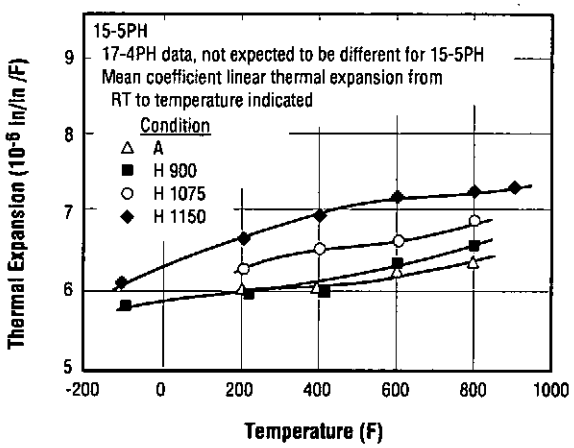

Figure 2.1.4 Thermal expansion (Refs. 1, 7, 27)

Table 2.1.5 Specific heat (Refs. 1, 7, 27)

Alloy	15-5PH[a]	
Condition	A	H 900
Specific Heat (32/212F) Btu/lb F	0.11	0.10

[a] 17-4PH data, not expected to be different for 15-5PH.

Table 2.2.1 Density (Refs. 1, 7, 27)

Alloy	15-5PH[a]			
Condition	A	H 900	H 1075	H 1150
Density (lb/cu in.) (gr/cu cm)	0.280 7.78	0.282 7.80	0.283 7.81	0.284 7.82

[a] 17-4PH data, not expected to be different for 15-5PH.

Table 2.2.2 Electrical resistivity (Refs. 1, 7, 27)

Alloy	15-5PH[a]	
Condition	A	H 900
Electrical Resistivity (microhm-inch)	38.5	30.3

[a] 17-4PH data, not expected to be different for 15-5PH.

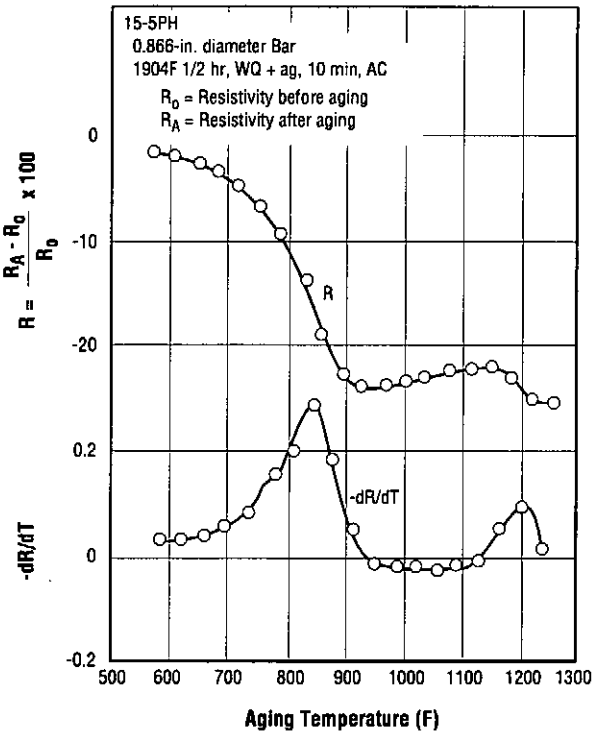

Figure 2.2.2.1 Effect of 10-minute aging temperature on change in electrical resistivity and its temperature derivative (Ref. 53)

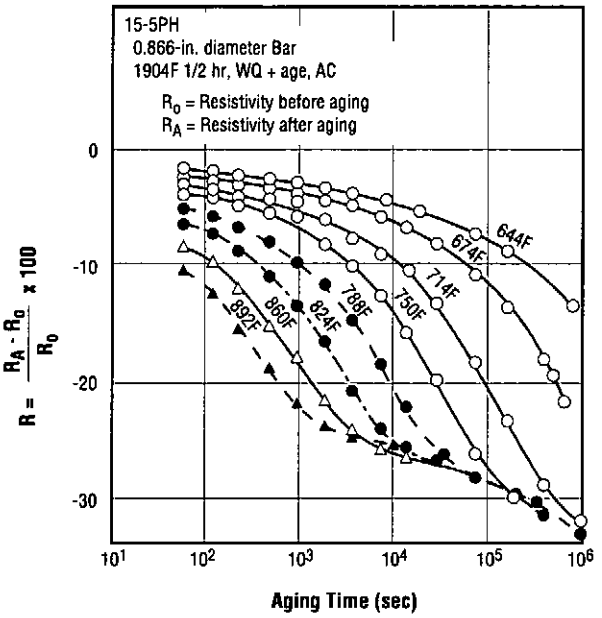

Figure 2.2.2.2 Effect of aging time on change in electrical resistivity over a range of aging temperatures (Ref. 53)

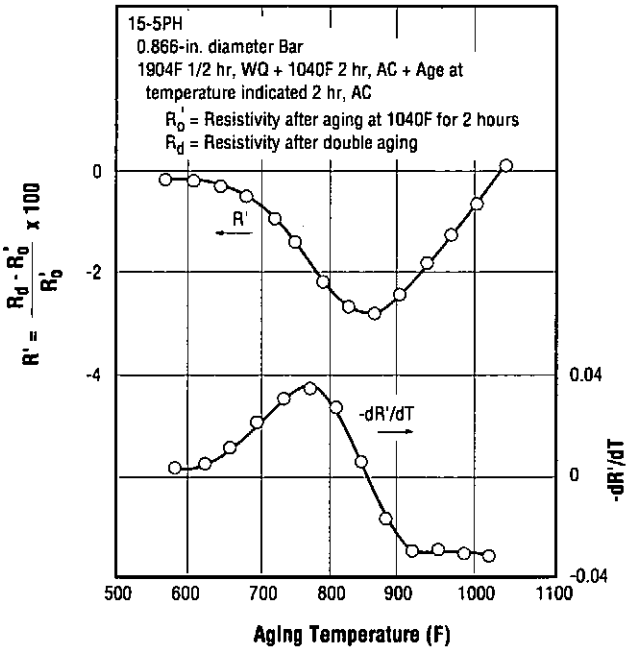

Figure 2.2.2.3 Effect of 2-hour aging temperature on electrical resistivity and its temperature derivative for specimens pre-aged at 1040F for 2 hours (Ref. 53)

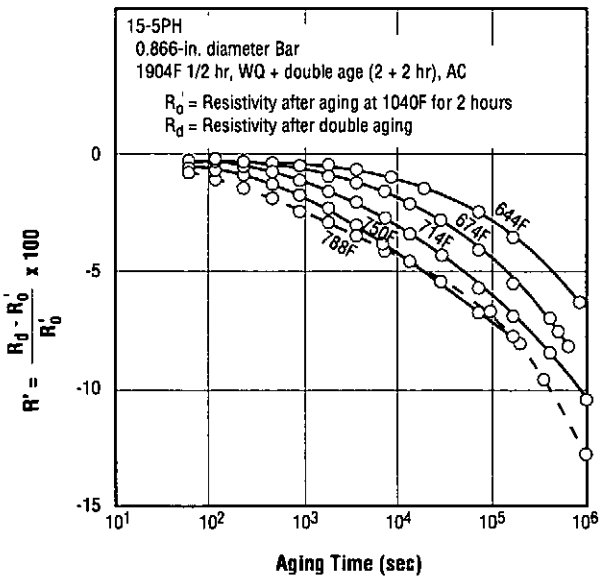

Figure 2.2.2.4 Effect of aging time on electrical resistivity for specimens aged at various temperatures subsequent to 1040F, 2 hour pre-age (Ref. 53)

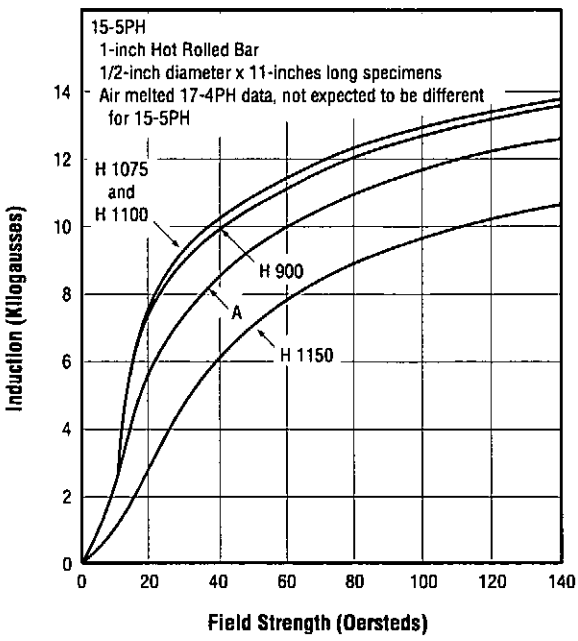

Figure 2.2.3.1 Induction curves (Ref. 10)

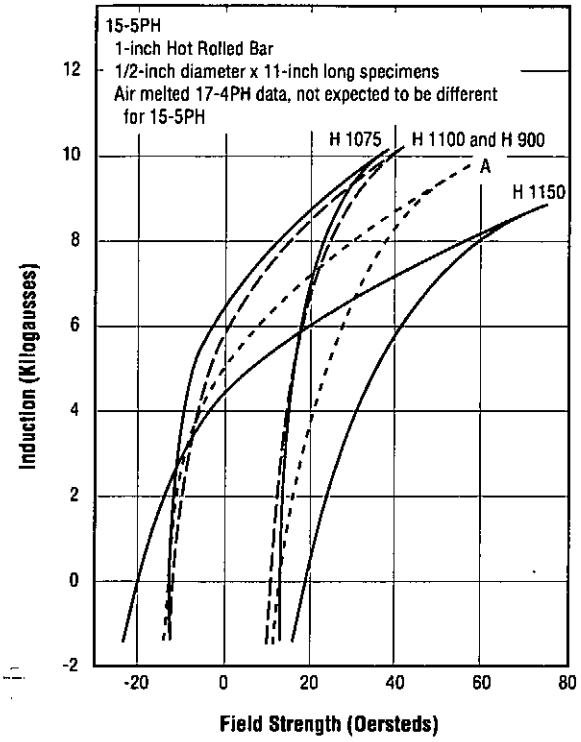

Figure 2.2.3.2 Hysteresis curves (Ref. 10)

Table 2.3.1.1 Corrosion of consumable electrode vacuum arc remelted 15-5PH and air melted 17-4PH in several corrosive media (Refs. 1, 12, 27)

Alloy	15-5PH	17-4PH
Form	1-inch Round Bar	
Condition	CVM	Air Melt
Boiling 65 percent HNO_3 - Average of five 48-hour periods[d]		
H 900	0.0083 IPM[a]	0.014 IPM
H 1025	0.0106 IPM	0.007 IPM
H 1150	0.0083 IPM	0.0065 IPM
1 percent HC1 at 95F - Average of five 48-hour periods[e]		
H 900	0.025 IPY[b]	0.035 IPY
H 1025	0.085 IPY	0.174 IPY
H 1150	0.730 IPY	0.650 IPY
Commercial Bleach - 7 days at 95F[e]		
H 900	0.0016 IPY	0.03 IPY
H 1025	0.013 IPY	0.03 IPY
H 1150	0.0083 IPY	0.03 IPY
5 percent Salt Fog at 95F - 10 days[f]		
H 900	No rust	5 - 10 percent rust
H 1025	0 - 5 percent rust[c]	10 - 25 percent rust
H 1150	0 - 5 percent rust	5 - 10 percent rust

[a] IPM = Inches per month.

[b] IPY = Inches per year.

[c] Percentage of total exposed area that rusted during test period.

[d] Tested according to ASTM Standard A 262.

[e] Tested according to ASTM Standard A 279.

[f] Tested according to ASTM Standard B 117.

Table 2.3.2.1 Stress corrosion cracking behavior of bar in three salt media (Refs. 60, 61)

a. Conventional tensile properties and salt spray and sea coast continuous exposure

Alloy	15-5PH					
Conventional Tensile Properties						
Heat (Reference)	Form	Condition	Test Direction	F_{tu} (ksi)	F_{ty} (ksi)	e (percent)
A (60)	3-in x 6-in Bar	H 1000 H 1050 H 1000 H 1050	ST ST LT LT	165 160 158 156	160 158 158 156	9 10 9 9
B (60)	3-in Diameter Bar	H 1000 H 1050	T T	169 162	164 158	14 16
C (60)	2 1/4-in x 6-in Bar	H 900 H 1000	ST ST	191 166	170 154	20 19
D (61)	2-in Diameter Bar	H 900 H 925 H 1025	L L L	189 187 164	173 163 156	11 11 9

Continuous Exposure[b]									
Heat (Reference)	Form	Condition	Test Direction	Applied Stress		5% Salt Spray		Sea Coast[a]	
				(ksi)	(% F_{ty})	F/N[c]	Exposure Time	F/N[c]	Exposure Time
A (60)	3-in x 6-in Bar	H 1000 H 1000 H 1000 H 1050 H 1050 H 1050 H 1000 H 1000 H 1000 H 1050 H 1050 H 1050	ST ST ST ST ST ST LT LT LT LT LT LT	80 120 160 79 119 158 79 119 158 78 117 156	50 75 100 50 75 100 50 75 100 50 75 100	0/4 0/3 0/3 0/3 0/3 0/3 0/3 0/3 0/3 0/3 0/3 0/3	6 mos	0/5	14 mos
B (60)	3-in Diameter Bar	H 1000 H 1000 H 1000 H 1050 H 1050 H 1050	T T T T T T	82 123 164 79 119 158	50 75 100 50 75 100	0/3	6 mos	0/5 0/4 0/4 0/5 0/4 0/4	14 mos
C (60)	2 1/4-in x 6-in Bar	H 900 H 900 H 1000 H 1000	ST ST ST ST	128 170 116 154	75 100 75 100	1/2 0/4	< 180 days 6 mos	0/5 2/5 0/5 0/5	14 mos 366, 384 days 14 mos 14 mos

Table 2.3.2.1 (cont'd) Stress corrosion cracking behavior of bar in three salt media (Refs. 60, 61)

b. Salt water alternate immersion

Alternate Immersion Exposure[d]							
Heat (Reference)	Form	Condition	Test Direction	Applied Stress		3.5% Salt Water Alternate Immersion[e]	
				(ksi)	(% F_{ty})	F/N[c]	Exposure Time
C (60)	2 1/4-in x 6-in Bar	H 900 H 1000	ST ST	170 154	100 100	2/2 0/4	156, 158 days 6 mos
D (61)	2-in Diameter Bar	H 900 H 900 H 925 H 925 H 1025 H 1025	L L L L L L	130 173 123 163 117 156	75 100 75 100 75 100	0/3	6 mos

[a] Kennedy Space Center.

[b] 1/8-inch diameter tensile specimens.

[c] F/N = ratio of failures to total number of specimens exposed.

[d] C-ring specimen.

[e] 10 minutes in solution; 50 minutes out of solution.

Table 2.3.2.2 Stress corrosion cracking of strip in marine atmosphere (Ref. 63)

Alloy		15-5PH				
Heat	Condition	F_{tu} (ksi)	F_{ty} (ksi)	Hardness (R_c)	Time (days) to Failure at	
					100% F_{ty} [a]	75% F_{ty} [a]
A	H 900	201	180	44.5	22, 22, 22	22, 22, 22
	H 925	187	172	42.5	22[b], 22[b], 266[b]	22[b], 22[b], 109[b]
	H 975	173	163	38.5	NF, NF, NF	NF, NF, NF
	H 1025	165	159	37.5	NF, NF, NF	NF, NF, NF
B	A	158	133	43.0	NF, NF, NF	NF, NF, NF
	H 900	196	173	44.5	21, 21, 21	21, 21, 26
	H 925	190	166	41.5	23[b], 23[b], 23[b]	23[b], 23[b], 23[b]
	H 975	170	159	39.5	NF, NF, NF	NF, NF, NF

[a] 1-inch x 8-inch x approximately 0.060-inch thick bent strip specimens exposed to a marine atmosphere on test racks facing the turf, tilted 30 degrees to the horizontal, located nominally 80 feet from the Atlantic Ocean at Kure Beach, North Carolina.

[b] Failure at stamped identification number near end of specimen.

[c] NF, no failures.

Table 2.3.2.3 Effect of aqueous salt environment and specimen orientation on stress corrosion cracking threshold, K_{Iscc} (Ref. 51)

Alloy-	15-5PH		
Condition	Environment	Orientation	K_{Iscc} (ksi $\sqrt{in.}$)
H 900	3.5% NaCl	LT	56
	20% NaCl	TL	33

Table 2.3.2.4 Tensile, plane strain fracture toughness, and stress corrosion cracking stress intensity factor in 3.5 percent aqueous salt solution for air melted and CVM billet in H 900 and H 1000 conditions (Ref. 64)

Alloy	15-5PH						
Form	Condition	F_{tu}[a] (ksi)	F_{ty}[a] (ksi)	e[a] (percent)	K_{Ic}[b] (ksi $\sqrt{in.}$)	K_{Iscc}[b,c] (ksi $\sqrt{in.}$)
3-in Sq Billet (Air Melt)	H 900 H1000	195.7 161.6	175.0 157.9	16 16	96.8[d] 114.0[d]	80.0 ± 2.0 114.0[e]
4 1/2-in Sq Billet (CVM)	H 900 H 1000	191.5 162.9	174.9 157.6	14 15	74.5 120.0[d]	55.8 ± 3.8 120.0

[a] L direction.

[b] LT crack plane orientation.

[c] In 3.5 NaCl aqueous solution.

[d] Not valid acording to ASTM E 399.

[e] No stress corrosion crack growth at stress intensity factor levels below approximately 85% K_Q.

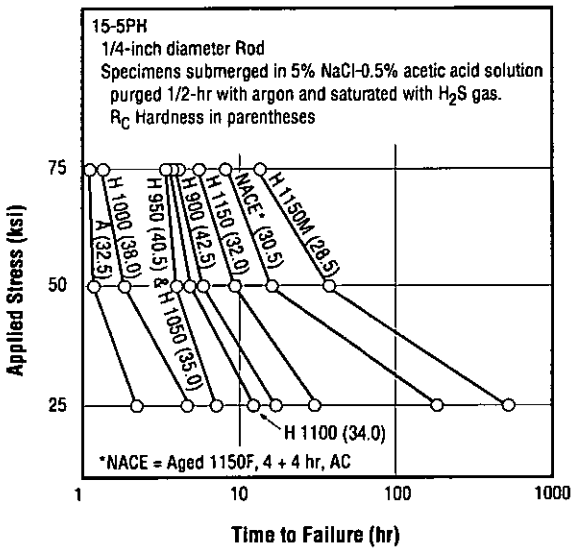

Figure 2.3.2.6 Sulfide stress corrosion cracking of rod (Ref. 62)

Table 3.1.1 Producer's guaranteed mechanical properties (Refs. 1, 2)

Alloy	15-5PH						
Form	See footnotes						
Condition	H 900	H 925	H 1025	H 1075	H 1100	H 1150	H 1150-M
Longitudinal Direction [a,b]							
F_{tu}, min (ksi)	190	170	155	145	140	135	115
F_{ty}, min (ksi)	170	155	145	125	115	105	75
e (2-in. or 4D) min (percent)	10	10	12	13	14	16	18
RA, min (percent)	35	38	45	45	45	50	55
Hardness, range, min (R_C)	40 - 47	38 - 45	35 - 42	31 - 39	32 - 38	28 - 37	24 - 30
Charpy-V Impact Energy, min (ft-lbs)	c	5	15	20	25	30	55
Transverse Direction[d]							
F_{tu}, min (ksi)	190	170	155	145	140	135	115
F_{ty}, min (ksi)	170	155	145	125	115	105	75
e (2-in. or 4D) min (percent)	6	7	8	9	10	11	14
RA, min (percent)	15	20	27	28	29	30	35
Hardness, range, min (R_C)	40 - 47	38 - 45	35 - 42	31 - 39	32 - 38	28 - 37	24 - 30
Charpy-V Impact Energy, min (ft-lbs)	c	c	10	15	15	20	35

[a] Intermediate location, (midway between center and edge).

[b] Air melted (up to 8-inch sections) or consumable electrode vacuum arc remelted (up to 12-inch sections).

[c] Minimum impact properties are not guaranteed in this condition.

[d] Consumable electrode vacuum arc remelted (up to 12-inch sections).

Table 3.1.2 AMS specified mechanical properties for air melted alloy products (Ref. 5)[a]

Alloy	15-5PH
Form	Bars, Wire, Forgings, Flash Welded Rings, and Stock for Forgings or Flash Welded Rings[b]
Condition	H 900
F_{tu}, min (ksi)	190
F_{ty}[c], min (ksi)	170
e (2-in. or 4D), min (percent)	10
RA, min (percent)	35
Hardness (BHN or equivalent)	388 - 448

[a] Reference 5 has been superseded by Reference 6.

[b] Up to 8-inch in section.

[c] 0.2 percent offset or 0.0159-inch extension in 2-inch gage length with $E = 28.5 \times 10^6$ psi.

Specimens taken in the longitudinal direction from bars and wire, from forgings with specimen axis approximately parallel to the forging flow lines, and in the circumferential direction from parent metal of flash welded rings.

Table 3.1.3 AMS specified mechanical properties for consumable electrode vacuum arc remelted alloy products (Ref. 6)

Alloy	15-5PH	
Form	Bars, Wire, Forgings, Flash Welded Rings, and Stock for Forgings or Flash Welded Rings[a]	
Condition	H 900	
	Longitudinal	Transverse
F_{tu}, min (ksi)	190	190
F_{ty}[b], min (ksi)	170	170
e (2-in. or 4D), min (percent)	10	6
RA, min (percent)	35	15
Hardness (BHN or equivalent)	388 - 444	

[a] Up to 12 inch in section.

[b] 0.2 percent offset or 0.0159-inch extension in 2-inch gage length with $E = 28.5 \times 10^6$ psi.

Longitudinal test requirements apply to specimens taken in the longitudinal direction from bars and wire, specimens taken from forgings with axis approximately parallel to the flow lines, and specimens taken in the circumferential direction from parent metal of flash welded rings; transverse test requirements apply to all other specimens.

Table 3.1.4 AMS and ASTM specified strength, hardness, and bendability of solution treated sheet, strip, and plate (Refs. 19, 23)

Alloy	15-5PH
Form	Sheet, Strip and Plate
Condition	A
Nominal Thickness (in.)	0.015 - 0.1875
F_{tu}, max (ksi)	185
F_{ty}, max (ksi)	160
e (2-in.), min (percent)	3
Hardness[a], max - R_C BHN	38 363
180 degree Bend Radius	18 x nominal thickness[b]

[a] Section thickness 0.0015 to 4.00 inch.

[b] Product nominal thickness 0.109-inch maximum.

Table 3.1.5 AMS and ASTM specified tensile strength and hardness for solution heat treated bars, forgings, flash welded rings, and wire (Refs. 6, 24, 25)

Alloy	15-5PH	
Form	Wire	Bars, Forgings, Flash Welded Rings, and Wire
Condition	A	
F_{tu}, max (ksi)	175	
Hardness[a], max R_C BHN or equivalent		38[b] 363[b]

[a] Hardness conversions are provided in ASTM E 140.

[b] For bars, determined at mid-radius or quarter thickness.

Table 3.1.6 AMS and ASTM specified tensile properties and hardness for precipitation hardened sheet, strip, and plate (Refs. 19, 23)

Alloy	15-5PH[a]					
Form	Sheet, Strip, and Plate[b]					
Condition	Nominal Thickness (in.)	F_{tu}, min (ksi)	F_{ty}, min (ksi)	e (2-in. or 4D), min (percent)	RA, min (percent)	Hardness, range [BHN (R_C)]
H 900	< 0.1875 0.1875 - 0.625 > 0.625 - 4.000	190	170	5 8 10	— 30 35	375-444 (40-47)
H 925	< 0.1875 0.1875 - 0.625 > 0.625 - 4.000	170	155	5 8 10	— 30 35	352-415 (38-45)
H 1025	< 0.1875 0.1875 - 0.625 > 0.625 - 4.000	155	145	5 8 12	— 35 40	331-388 (35-42)
H 1075	< 0.1875 0.1875 - 0.625 > 0.625 - 4.000	145	125	5 9 13	— 35 45	311-363 (33-39)
H 1100	< 0.1875 0.1875 - 0.625 > 0.625 - 4.000	140	115	5 10 14	— 35 45	302-352 (32-38)
H 1150	< 0.1875 0.1875 - 0.625 > 0.625 - 4.000	135	105	8 10 16	— 40 50	269-341 (28-37)

[a] Multiple melted using vacuum-arc consumable electrode or electroslag processes in the final melting cycle.

[b] Products thickness 4.0 inch maximum.

Table 3.1.7 AMS and ASTM specified tensile properties and hardness for precipitation hardened bars, forgings, flash welded rings extrusions, and stock for forging, flash welded rings, or extruding (Refs. 6, 24, 25)

Alloy	15-5PH[a]					
Form	Bars, Forgings, Flash Welded Rings, Extrusions, and Stock[b] for Forging, Flash Welded Rings, or Extruding					
Condition	H 900	H 925	H 1025	H 1075	H 1100	H 1150
Longitudinal						
F_{tu}, min (ksi)	190	170	155	145	140	135
F_{ty}, min (ksi)	170	155	145	125	115	105
e (2-in. or 4D), min (percent)	10	10	12	13	14	16
RA, min (percent)	35	38	45	45	45	50
Hardness, range (BHN)	388 - 444	375 - 429	331 - 401	311 - 375	302 - 363	277 - 352
Transverse[c]						
F_{tu}, min (ksi)	190	170	155	145	140	135
F_{ty}, min (ksi)	170	155	145	125	115	105
e (2-in. or 4D), min (percent)	6	10	8	9	10	11
RA, min (percent)	20[d]	25[e]	32[f]	33[g]	34[h]	35
Hardness, range (BHN)	388 - 444	375 - 429	331 - 401	311 - 375	302 - 363	277 - 352

[a] Multiple melted using vacuum consumable electrode practice during remelting or multiple melted using electroslag process in the final melting cycle.

[b] Property specification applies to stock forged to a test coupon and heat treated. Tests on coupons taken from forged stock after heat treatment shall be accepted as equivalent to tests of a heat treated forged coupon.

[c] Transverse tensile property requirements apply only to products from which a test specimen not less than 2-1/2 inch long or 1/2-inch x 1/2-inch cross-section can be extracted.

[d] ASTM (25) specifies RA, min = 15 percent.

[e] ASTM (25) specifies RA, min = 20 percent.

[f] ASTM (25) specifies RA, min = 27 percent.

[g] ASTM (25) specifies RA, min = 28 percent.

[h] ASTM (25) specifies RA, min = 30 percent.

Table 3.1.8 AMS specified tensile properties and hardness for precipitation hardened investment castings (Refs. 13 - 17)

Alloy	15-5PH			
Form	Investment Castings			
Source	AMS (13, 16)	AMS (16, 17)	AMS (14, 16)	AMS (15, 16)
Condition	H 925	H 935	H 1000	H 1100
Separately Cast Specimens				
F_{tu}, min (ksi)	180	170	150	130
F_{ty}, min (ksi)	160	150	130	120
e (4D), min (percent)	6	7	8	8
RA, min (percent)	15	16	18	20
Hardness, range (R_C)	40 - 44	38 - 47	35 - 42	33 - 40
Integrally Cast Specimens or Specimens Machined From Castings				
F_{tu}, min (ksi)	180	170	150	130
F_{ty}, min (ksi)	160	150	130	120
e (4D), min (percent)	5	6	8	6
RA, min (percent)	12	14	15	18
Hardness, range (R_C)	40 - 44	38 - 47	35 - 42	33 - 40

Separately cast and integrally cast tensile specimens may be either cast to size, or cast oversize and subsequently machined to required 0.250-inch diameter.

Table 3.1.9 AMS specified tensile properties and hardness for precipitation hardened tubular centrifugal castings (Ref. 18)

Alloy	15-5PH
Form	Tubular Centrifugal Castings
Condition	H 925
F_{tu}, min (ksi)	180
F_{ty}, min (ksi)	150
e (4D), min (percent)	6
RA, min (percent)	15
Hardness, range (R_C)	40 - 45

Table 3.1.10 Producer's specified acceptable tensile properties and hardness for Condition A (Refs. 1, 27)

Alloy	15-5PH				
Form	Rounds, Hexagons, and Squares			Flats	Sheet and Strip
Condition	A				
Size	≤ 1/8 inch	> 1/8 inch to 1/2 inch	> 1/2 inch	> 1/2 inch	all
F_{tu} (ksi)	175 max	—	—	—	185 max
F_{ty} (ksi)	—	—	—	—	160 max
e (2-in.), (percent)	—	—	—	—	3 min
Hardness	—	R_C 38 max	BHN 363 max	BHN 363 max	R_C 38 max

Note: See Section 1.9.4.

Table 3.1.11 Producer's specified acceptable tensile properties and hardness for sheet and strip in H Conditions (Ref. 27)

Alloy	15-5PH					
Form	Sheet and Strip					
Condition	H 900	H 925	H 1025	H 1075	H 1100	H 1150
F_{tu}, min (ksi)	190	170	155	145	140	135
F_{ty}, min (ksi)	170	155	145	125	115	105
e (2-in.), min (percent)	5	5	5	5	5	8
Hardness, range (R_C)	40 - 48	38 - 46	35 - 43	31 - 40	31 - 40	28 - 38

Table 3.2.1.1 Typical mechanical properties for bar (Refs. 1, 7)

Alloy	15-5PH						
Form	Up to 12-inch Sections						
Condition	H 900	H 925	H 1025	H 1075	H 1100	H 1150	H 1150-M
Longitudinal Direction - Intermediate Location Air Melted or Consumable Electrode Vacuum Arc Remelted							
F_{tu} (ksi)	200	190	170	165	150	145	125
F_{ty} (ksi)	185[a]	175	165	150	135	125	85
e (2-in. or 4D), (percent)	14	14	15	16	17	19	22
RA (percent)	50	54	56	58	58	60	68
Hardness (BHN) (R_C)	420 44	409 42	352 38	341 36	332 34	311 33	277 27
Charpy-V Impact Energy (ft-lbs) RW or RT Direction	15	25	35	40	45	50	100
Transverse Direction - Intermediate or Center Location Consumable Electrode Vacuum Arc Remelted							
F_{tu} (ksi)	200	190	170	165	150	145	125
F_{ty} (ksi)	185	175	165	150	135	125	85
e (2-in. or 4D), (percent)	10	11	12	13	14	15	18
RA (percent)	30	35	42	43	44	45	50
Hardness (BHN) (R_C)	420 44	409 42	352 38	341 36	332 34	311 33	277 27
Charpy-V Impact Energy[b] (ft-lbs) TW or WT Direction TR or WR Direction	7 8	17 12	27 25	30 25	30 25	50 45	100 70

[a] For condition H 900, F_{cy} = 178 ksi.

[b] For intermediate location only.

Table 3.2.1.2 Typical mechanical properties for sheet and strip (Ref. 27)

Alloy	15-5PH						
Form	Sheet and Strip - Cold Flattened						
Condition	A	H 900	H 925	H 1025	H 1075	H 1150	H 1150-M
Longitudinal							
F_{tu} (ksi)	161	209	181	174	162	150	136
F_{ty} (ksi)	140	201	175	171	160	140	111
e (2-in.), (percent)	8.4	10.1	12.2	12.2	12.8	14.6	18.8
Hardness (R_C)	35	46	41	40	38	36	31
Transverse							
F_{tu} (ksi)	162	213	184	175	162	152	137
F_{ty} (ksi)	143	202	177	171	161	146	111
e (2-in.), (percent)	7.6	9.4	9.8	9.3	11.4	13.1	17.8
Hardness (R_C)	35	46	42	39	38	36	0.

Average of two heats.

0.090-inch gage.

Table 3.2.1.3 Effects of section size, specimen location and specimen direction on tensile properties of arc melted and vacuum remelted stock in H 900 Condition (Ref. 3)

Alloy	15-5PH						
Form	Large Rectangular Forged Sections						
Condition	H 900						
Melting Method	Section Size (in)	Direction	Location[a]	F_{tu} (ksi)	F_{ty} (ksi)	e (4D), (percent)	RA (percent)
Arc Air	12 x 14	ST	E	188	172	11	36
			I				32
			C	186	176	4	9
Vacuum Remelted	12 x 14	ST	E	186	172	11	34
			I		174		35
			C		170		32
	3 x 5 1/2	L	I	188	187	15	54
		ST	C	189	—	14	46
	3 1/2 x 12	L	I	187	185	15	50
		ST	C	190	—	14	48
	3 1/2 x 15 1/2	L	I	193	190	11	40
		ST	C		192	8	28
	4 x 24	L	I	194	189	12	40
		ST	C				36

[a] E = edge; I = intermediate; C = center.

Table 3.2.1.4 Room temperature tension, compression, shear, and bearing properties of plate in H 1025 condition, for which fatigue properties appear in Figures 3.5.1.6 and 3.5.1.7 (Ref. 32)

Alloy	15-5PH		
Form	0.215 - 2.579-in. Plate		
Condition	H 1025[a]		
Direction	L	T	ST
F_{tu} (ksi)	171.0	171.4	—
F_{ty} (ksi)	165.6	166.0	—
RA (percent)	58.5	57.6	—
e (2-in.) (percent)	15.0	14.8	—
E_t (1000 ksi)	28.66	28.72	—
F_{cy} (ksi)	175.6	175.3	174.9[b]
E_c (1000 ksi)	29.85	29.84	30.03[b]
F_{su}[c] (ksi)	114.3	113.2	—
F_{su}[d] (ksi)	108.1	109.0	—
e/D = 1.5			
F_{bru} (ksi)	287.3	287.2	—
F_{bry} (ksi)	246.1	246.3	—
e/D = 2.0			
F_{bru} (ksi)	368.4	367.8	—
F_{bry} (ksi)	286.7	289.1	—

[a] Values average of triplicate tests.

[b] Results from two heats, plate thickness > 1.5 inch.

[c] Full thickness tests from three heats (plates), for which plate thickness < 3.0 inch.

[d] 0.25-inch diameter double pin shear tests from seven heats (plates), for which plate thickness > 3.0 inch.

Table 3.2.5.1 Shear strength in torsion (Refs. 1, 7)

Alloy	15-5PH[a]			
Condition	H 900	H 1025	H 1075	H 1150
Torsional Shear Strength at Elastic Limit (ksi)	98.0	86.2	67.5	42.5
Ultimate Torsional Shear Strength (Modulus of Rupture) (ksi)	171.0	141.0	135.0	124.0

[a] 17-4PH data, not expected to be different for 15-5PH.

Table 3.2.5.2 Shear strength in double shear for H 900 condition (Ref. 1)

Alloy	15-5PH	
Condition	H 900	
Specimen Size	F_{su} (ksi)	F_{tu} (ksi)
5/8-inch round	133.0	192.0
1/2-inch round	130.0	
1/4-inch round	133.5	

17-4PH data, not expected to be different for 15-5PH.

Tests conducted in accordance with the National Aircraft Standard No. 498.

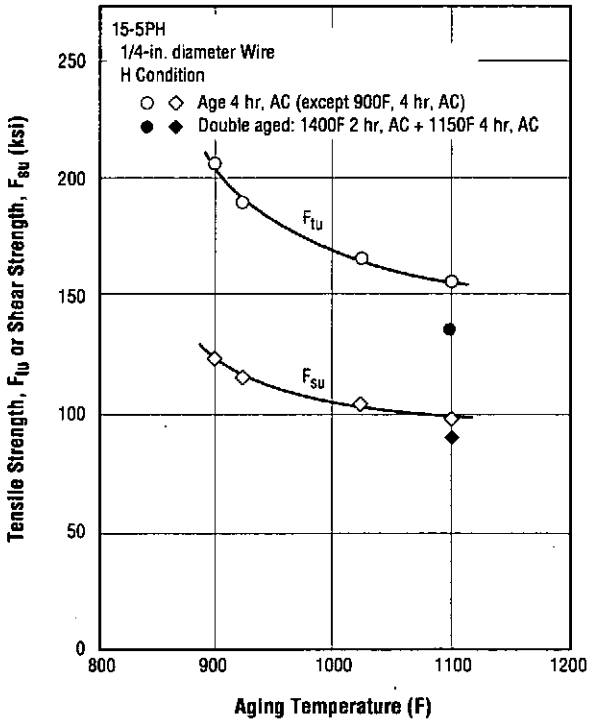

Figure 3.2.5.3 Effect of aging temperature (H condition) on shear strength in double shear (Ref. 49)

Table 3.2.6.1 Bearing strength of plate in H 1025 condition (Refs. 32, 65)

Alloy	15-5PH					
Condition	H 1025					
	Ratio of Edge Distance to Hole Diameter		e/D = 1.5		e/D = 2.0	
Source	Heat/Form	Test Direction	F_{bru} (ksi)	F_{bry} (ksi)	F_{bru} (ksi)	F_{bry} (ksi)
Ref. 32	0.215 - 2.579-in. Plate	L	287.3	246.1	368.4	286.7
		T	287.2	246.3	367.8	289.1
Ref. 65	A/ 1 1/2 x 5-in Flat Bar	L	280.5	234.1	364.7	281.7
	B/ 5/8 x 2-in. Flat Bar	L	274.1	229.0	355.4	275.8
	C/ 5/8 x 2-in. Flat Bar	L	281.1	238.3	363.1	276.9

Table 3.2.6.2 Bearing strength of bar in H 1150 condition (Ref. 65)

Alloy		15-5PH			
Condition		H 1025			
Ratio of Edge Distance to Hole Diameter		e/D = 1.5		e/D = 2.0	
Heat/Form	Test Direction	F_{bru} (ksi)	F_{bry} (ksi)	F_{bru} (ksi)	F_{bry} (ksi)
A/ 5 1/2-in. Dia Cylindrical Bar	L	228.9	179.6	294.8	221.1
	T	227.1	178.7	292.3	215.2
B/ 1 1/2 x 5-in Flat Bar	L	233.9	186.4	297.6	224.6
	T	231.3	180.6	290.9	220.8
C/ 1 1/2 x 7.7-in. Flat Bar	L	235.6	190.0	301.5	224.0
	T	237.9	185.8	301.6	226.6
D/ 1 1/2 x 3-in. Flat Bar	L	231.6	182.6	295.9	222.3
E/ 5/8 x 2-in. Flat Bar	L	230.9	177.0	296.4	213.8
F/ 5/8 x 2-in. Flat Bar	L	238.1	188.2	298.4	224.6

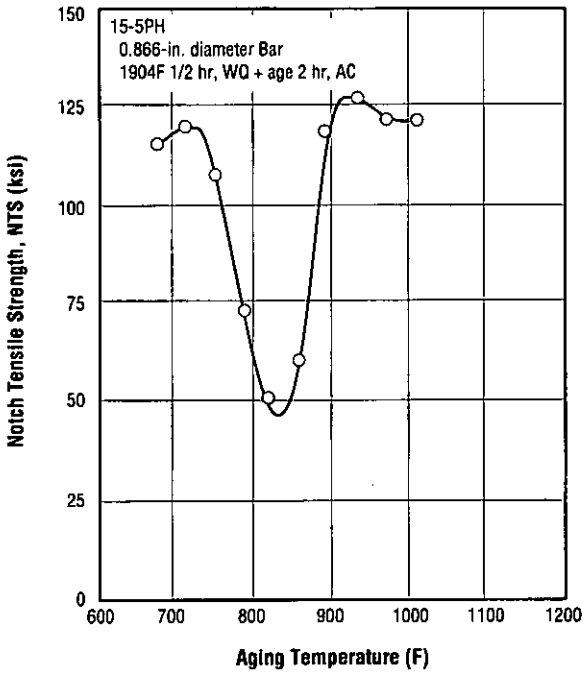

Figure 3.2.7.1.3 Effect of aging temperature on notch tensile strength of bar (Ref. 53)

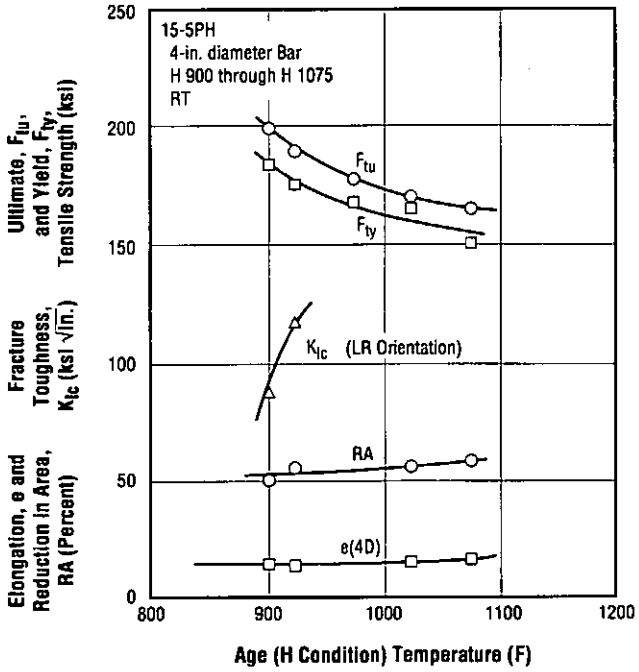

Figure 3.2.7.2.1 Effect of age (H condition) temperature on tensile properties and plane strain fracture toughness (Ref. 40)

Table 3.2.7.2.4 J-integral fracture toughness of plate and weldment (Ref. 48)

Alloy		15-5PH		
Form	Condition	Crack Plane Orientation	J_{Ic} (kN/m)	Effective[a] F_{ty} (MPa)
Plate	ST + Age	TL	192 - 238	1100
Weld[b]	As-welded	—	107 - 124	1050
	Weld + Age	—	76 - 156	1220
	Weld + ST + Age	—	157 - 157	1200

[a] $(F_{ty} + F_{tu})/2$

[b] AMS 5826.

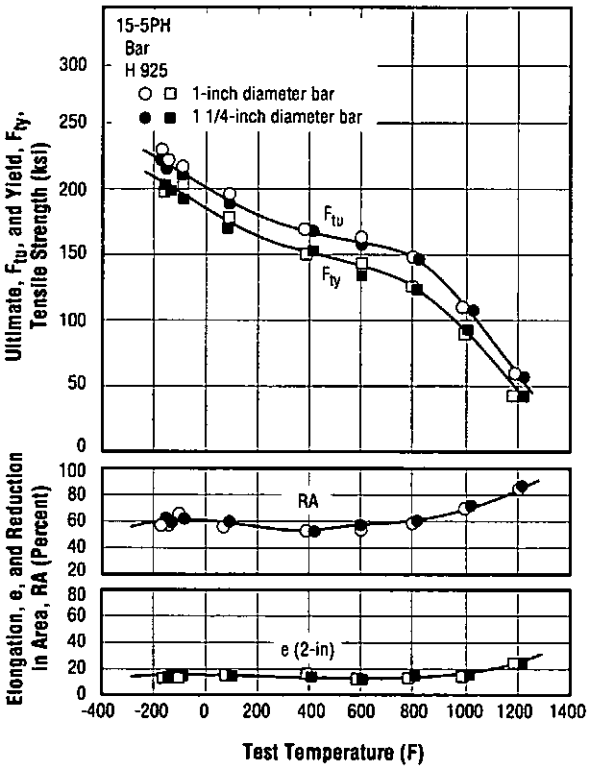

Figure 3.3.1.1 Effect of test temperature on tensile properties of bar in H 925 condition (Ref. 29)

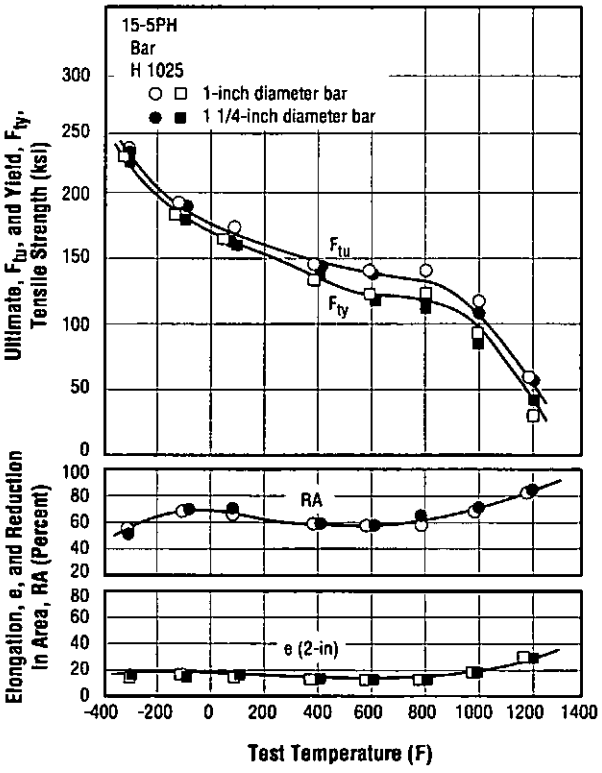

Figure 3.3.1.2 Effect of test temperature on tensile properties of bar in H 1025 condition (Ref. 29)

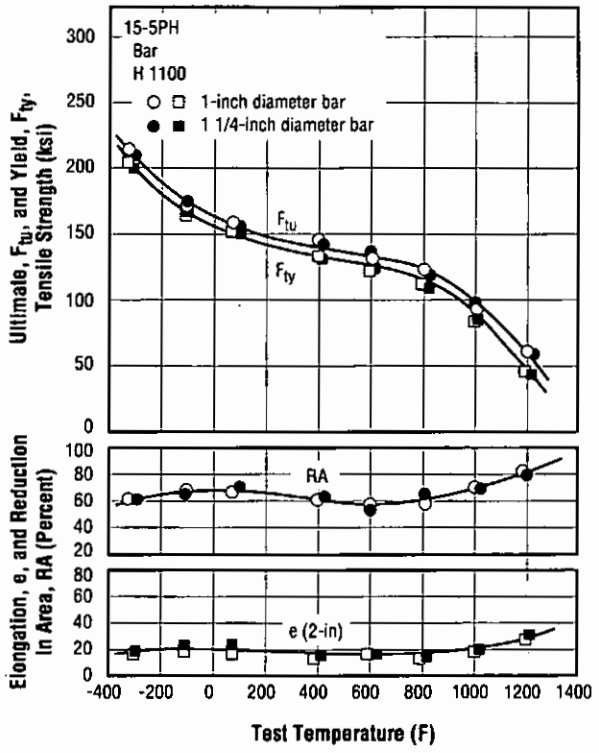

Figure 3.3.1.3 Effect of test temperature on tensile properties of bar in H 1100 condition (Ref. 29)

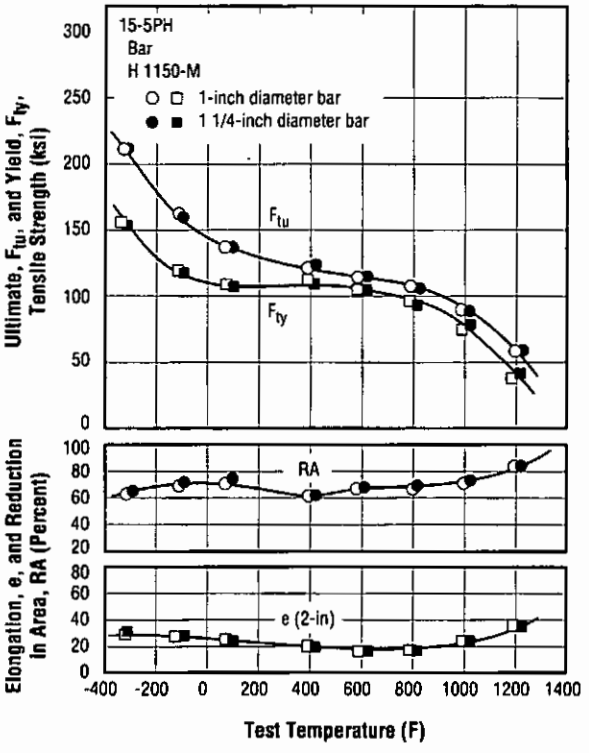

Figure 3.3.1.4 Effect of test temperature on tensile properties of bar in H 1150-M condition (Ref. 29)

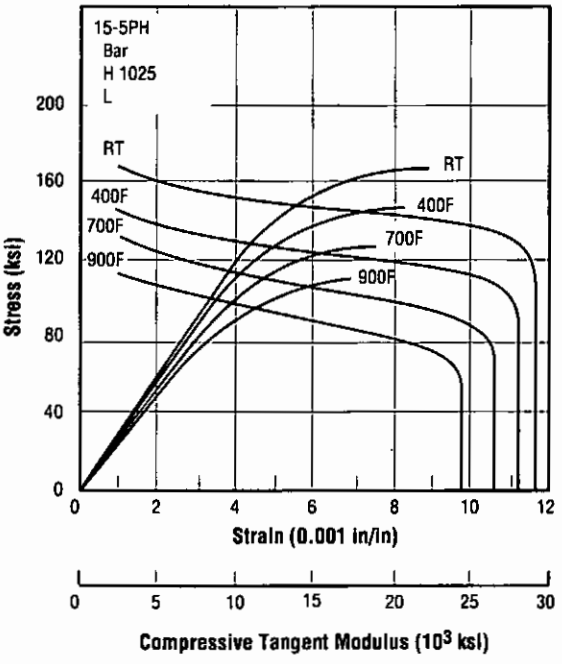

Figure 3.3.2.1 Typical compressive stress-strain and tangent-modulus curves at selected temperatures for bar in H 1025 condition (Ref. 65)

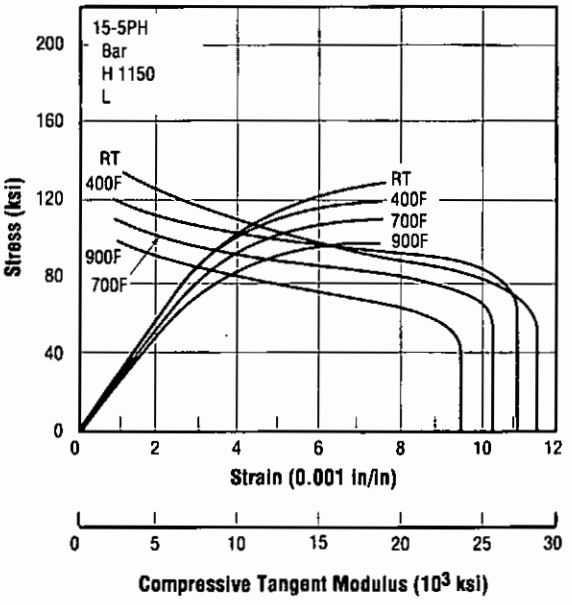

Figure 3.3.2.2 Typical compressive stress-strain and tangent-modulus curves at selected temperatures for bar in H 1150 condition (Ref. 65)

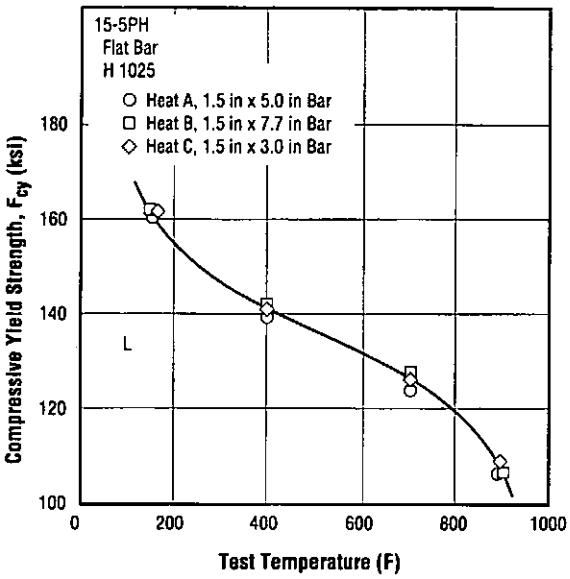

Figure 3.3.2.3 Effect of test temperature on compressive yield strength of bar in H 1025 condition (Ref. 65)

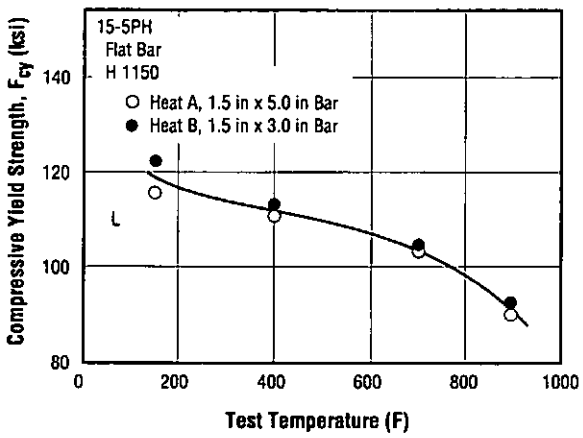

Figure 3.3.2.4 Effect of test temperature on compressive yield strength of bar in H 1150 condition (Ref. 65)

Table 3.3.3.1 Charpy-V impact energy for sheet at room temperature and -65F (Ref. 27)

Alloy	15-5PH	
Form	0.093-inch thick	
Condition	Charpy-V Impact Energy[a,b] (in-lbs)	
	RT	-65F
A	3265	2669
H 900	2857	2361
H 1025	3974	3378
H 1150	4626	4248
H 1150-M	5616	5049

[a] Each value average triplicate tests for two heats.

[b] Charpy-V specimens: B = 0.093 inch, (W-a) = 0.314 Inch.

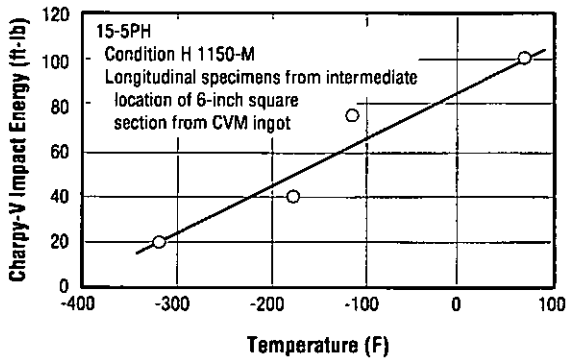

Figure 3.3.3.2 Effect of temperature on Charpy-V impact energy for Condition H 1150-M (Refs. 1, 2)

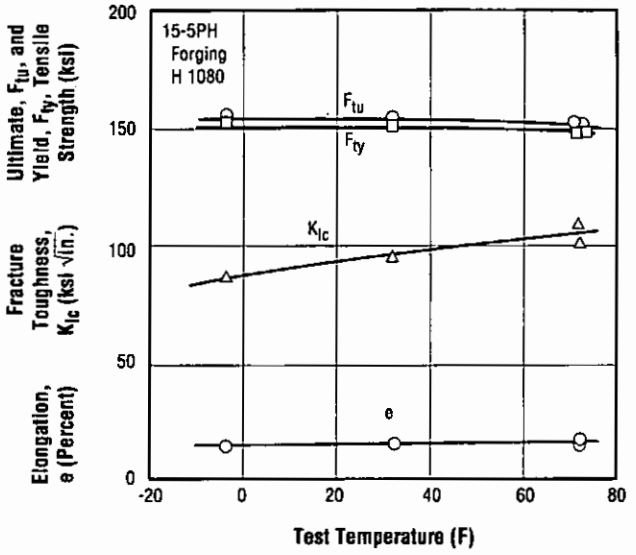

Figure 3.3.7.2.1 Effect of test temperature in the range -4 to 72F on the tensile properties and plane strain fracture toughness (Ref. 44)

Table 3.3.7.2.2 Effect of aged condition, test temperature, and specimen orientation on strength and plane strain fracture toughness (Ref. 51)

Alloy	15-5PH				
Condition	Test Temperature (F)	Orientation	F_{tu} (ksi)	F_{ty} (ksi)	K_{Ic} (ksi $\sqrt{in.}$)
H 900	RT	LT	200	185	87
		—	192	175	74
		TL	193	171	74
H 1080	72	Random	151	149	104 - 111
	32		152	151	87 - 104
	-4		153	151	81 - 92

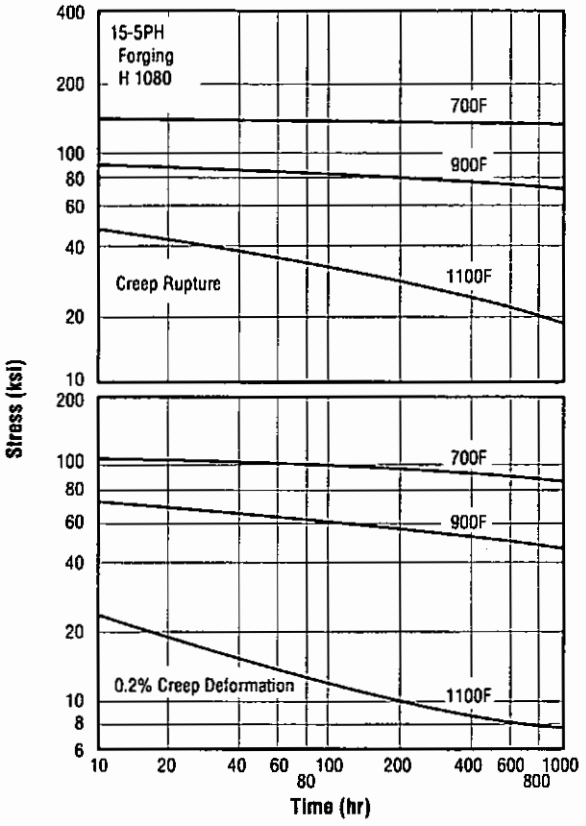

Figure 3.4.1 Creep deformation and rupture curves at selected temperatures for forged bar in the H 1025 condition (Ref. 66)

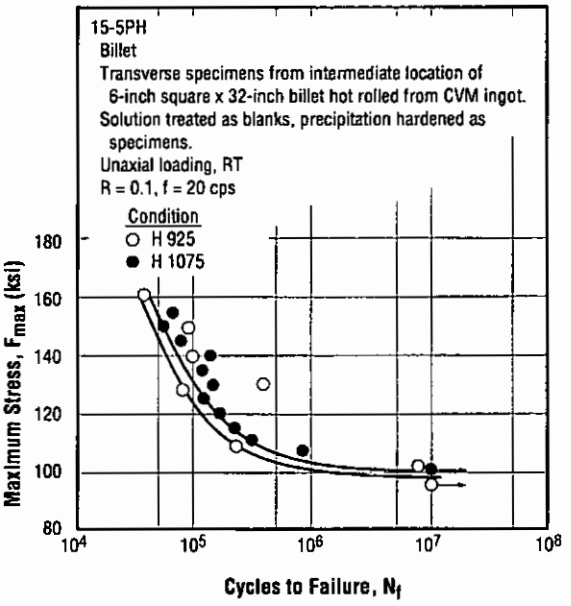

Figure 3.5.1.1 Room temperature axial-load fatigue strength of CVM billet in H 925 and H 1075 (Ref. 1)

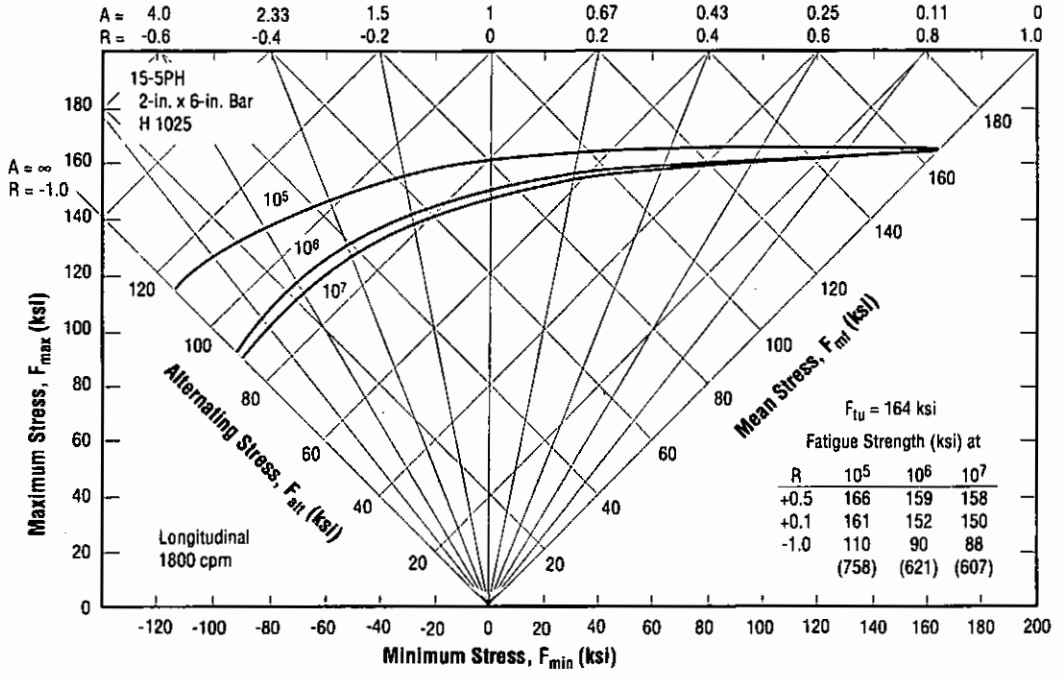

Figure 3.5.1.2 Room temperature longitudinal unnotched axial-load constant-life fatigue diagram for bar (Ref. 56)

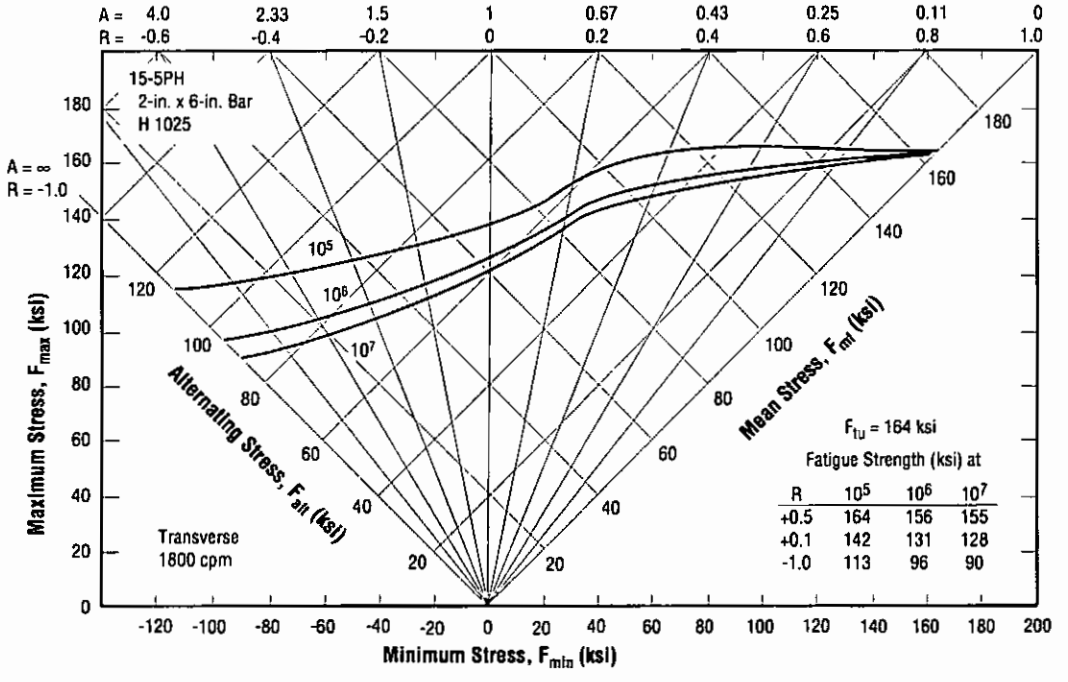

Figure 3.5.1.3 Room temperature transverse unnotched axial-load constant-life fatigue diagram for bar (Ref. 56)

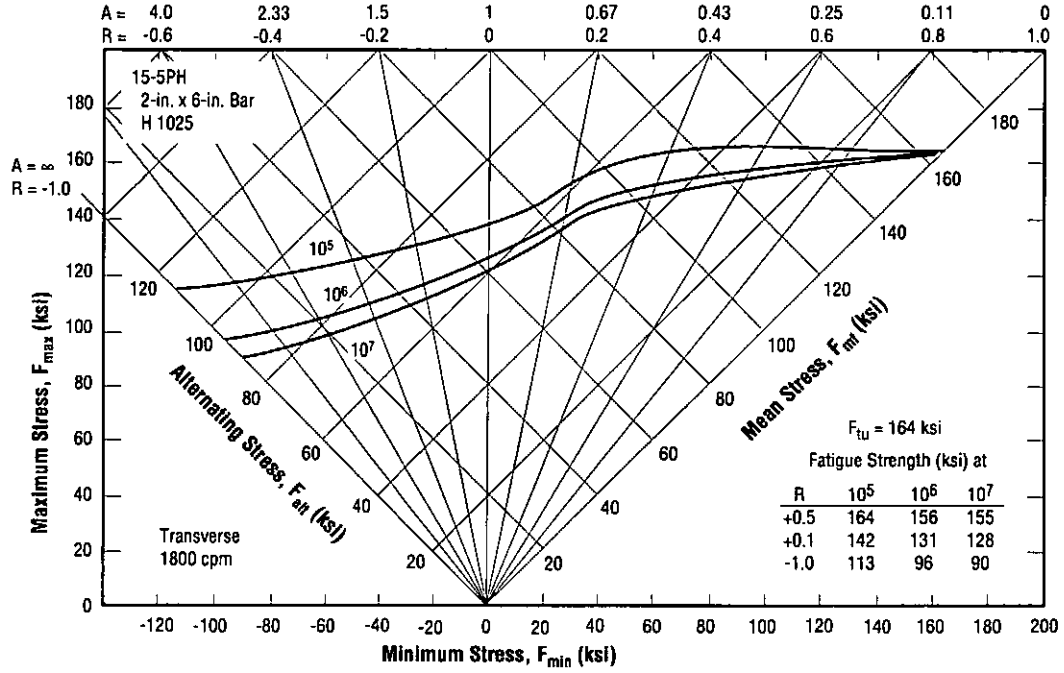

Figure 3.5.1.3 Room temperature transverse unnotched axial-load constant-life fatigue diagram for bar (Ref. 56)

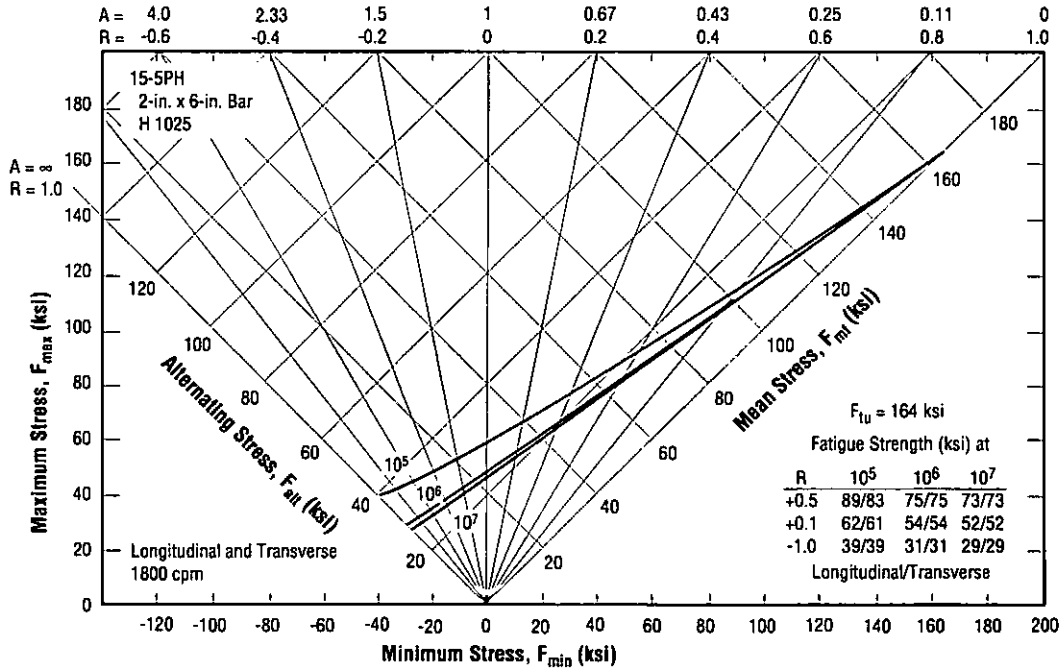

Figure 3.5.1.4 Room temperature longitudinal and transverse notched (K_t = 3.0) axial-load constant-life fatigue diagram for bar (Ref. 56)

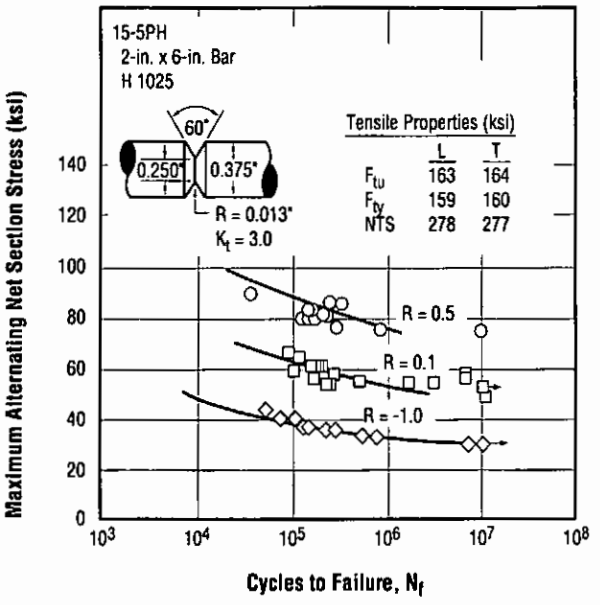

Figure 3.5.1.5 Mild-notch axial-load fatigue strength of bar in H 1025 condition at stress ratios, R = 0.5, 0.1, and -1.0 (Ref. 55)

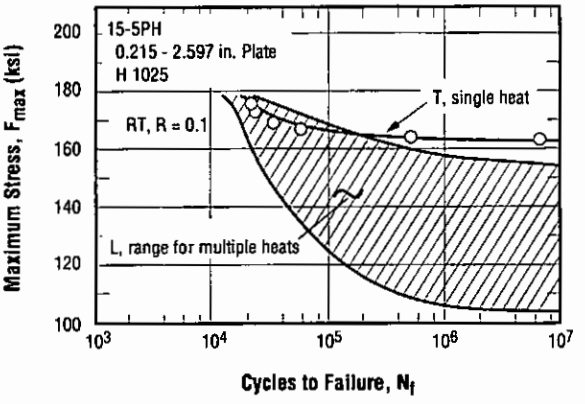

Figure 3.5.1.6 Room temperature axial-load fatigue strength of plate in H 1025 condition (Ref. 32)

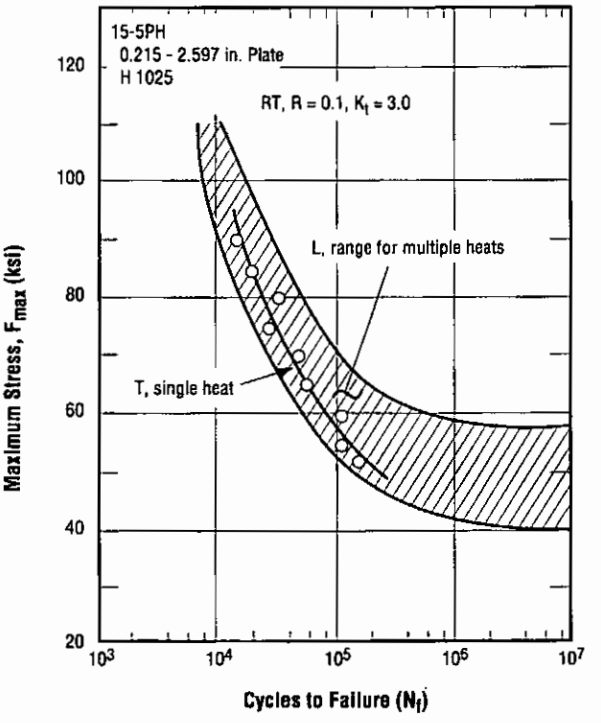

Figure 3.5.1.7 Room temperature axial-load notched (K_t = 3.0) fatigue strength of plate in H 1025 condition (Ref. 32)

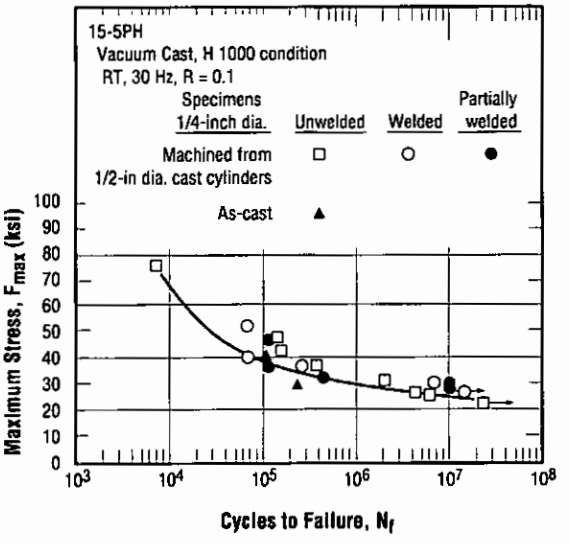

Figure 3.5.1.8 Room temperature axial-load high-cycle fatigue strength of machined and as-cast specimens from welded and unwelded vacuum castings (Ref. 26)

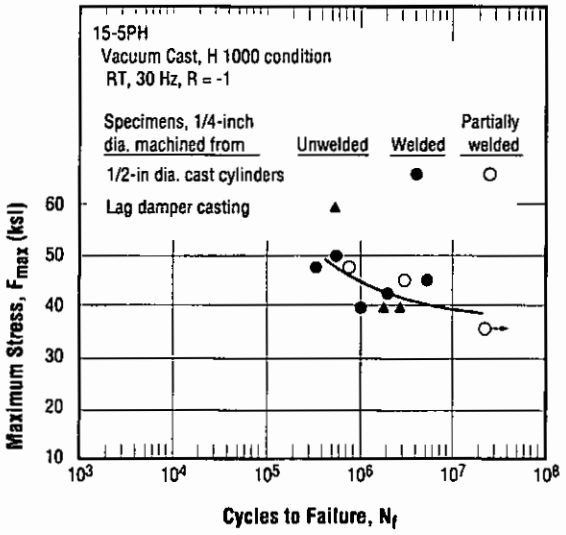

Figure 3.5.1.9 Room temperature tension-compression high-cycle fatigue strength of specimens machined from cast cylinders and from a lag damper casting (Ref. 26)

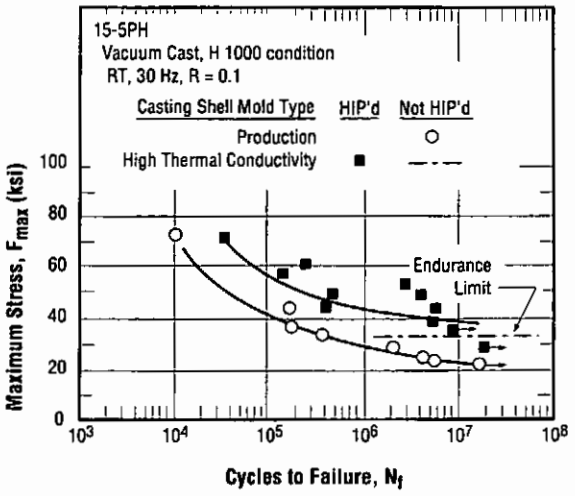

Figure 3.5.1.10 Room temperature axial-load high-cycle fatigue strength of specimens machined from bars vacuum cast into either production or high thermal conductivity shell molds, and subsequently HIP'd or not HIP'd (Ref. 26)

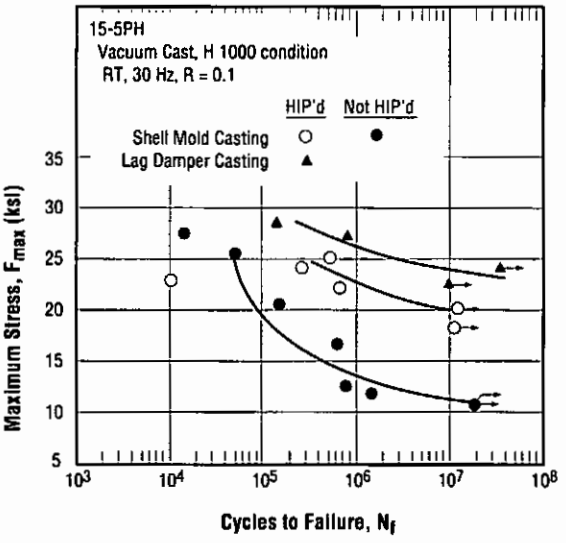

Figure 3.5.1.11 Room temperature axial-load high-cycle fatigue strength of HIP'd and not HIP'd notched (K_t = 3.0) specimens machined from shell mold castings and notched (K_t = 3.0) specimens machined from HIP'd lag damper casting (Ref. 26)

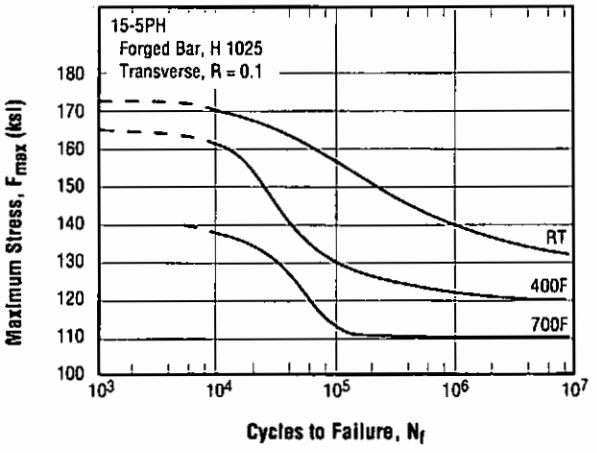

Figure 3.5.1.12 Elevated temperature transverse unnotched axial-load fatigue strength of forged bar (Ref. 56)

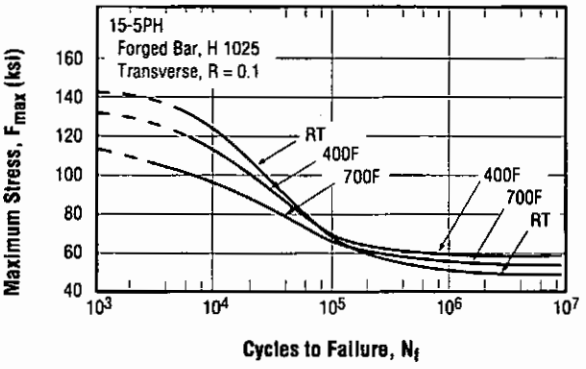

Figure 3.5.1.13 Elevated temperature transverse notched (K_t = 3.0) axial-load fatigue strength of forged bar (Ref. 56)

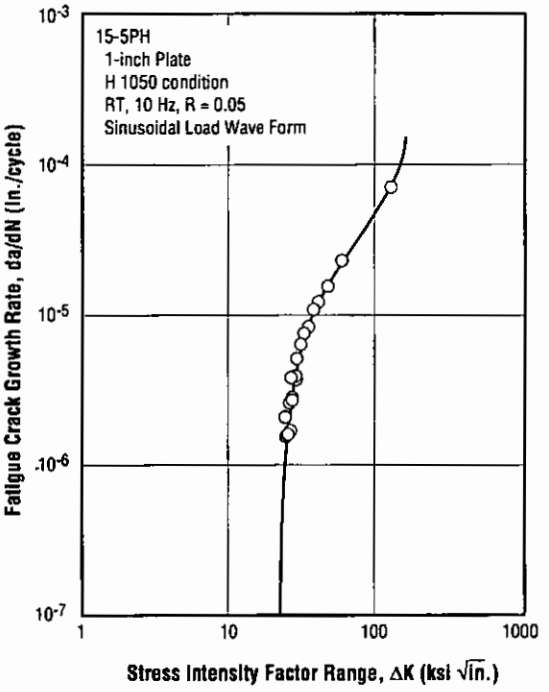

Figure 3.5.3.1 Room temperature fatigue crack growth rate at 10 Hz, R = 0.05 for plate in H 1050 condition (Ref. 28)

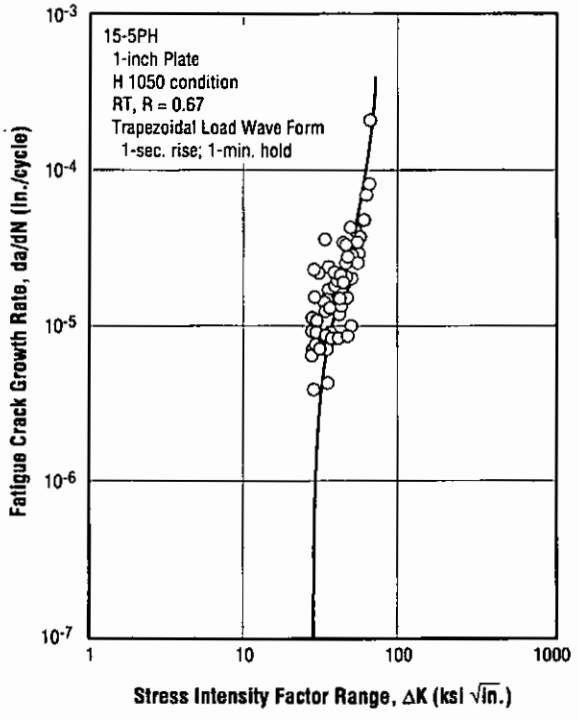

Figure 3.5.3.2 Room temperature fatigue crack growth rate at R = 0.67, trapezoidal load wave form (1-minute hold time), for plate in H 1050 condition (Ref. 28)

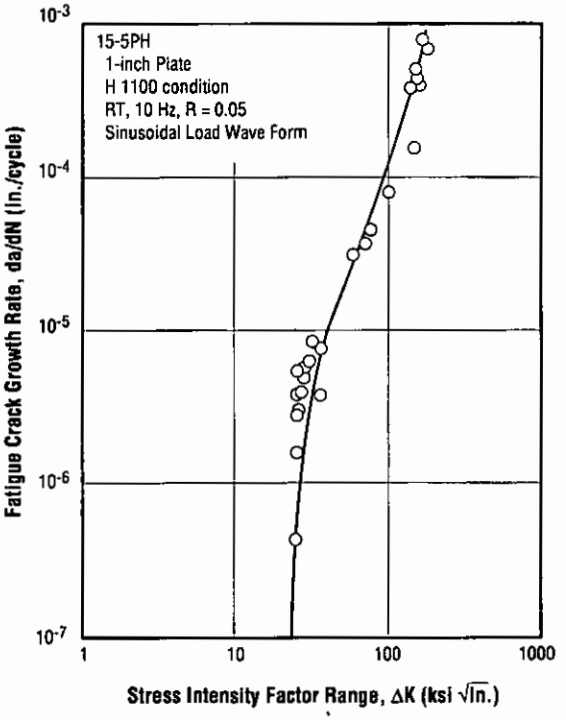

Figure 3.5.3.3 Room temperature fatigue crack growth rate at 10 Hz, R = 0.05, for plate in H 1100 condition (Ref. 28)

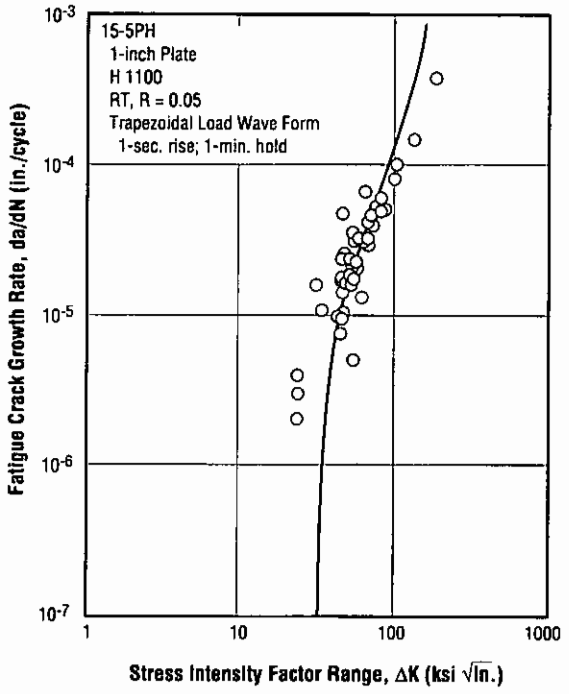

Figure 3.5.3.4 Room temperature fatigue crack growth rate at R = 0.05, trapezoidal load wave form (1-minute hold time), for plate in H 1100 condition (Ref. 28)

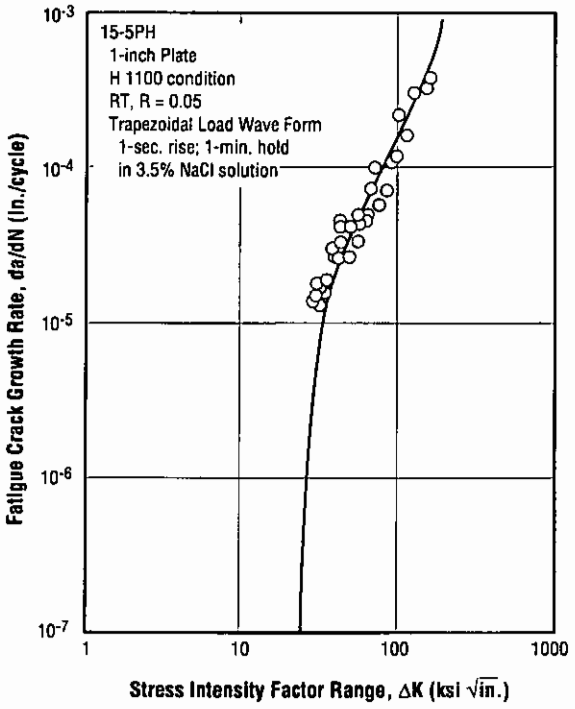

Figure 3.5.3.5 Room temperature fatigue crack growth rate in 3.5 percent NaCl solution at R = 0.05, trapezoidal load wave form (1-minute hold time), for plate in H 1100 condition (Ref. 28)

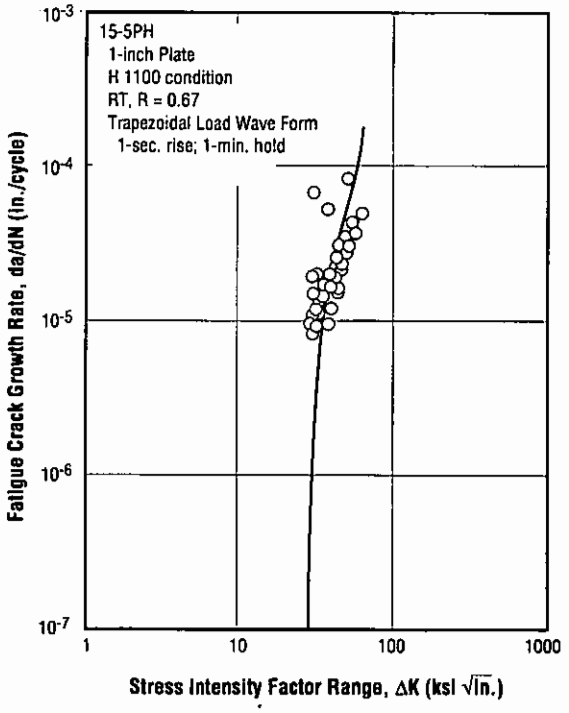

Figure 3.5.3.6 Room temperature fatigue crack growth rate at R = 0.67, trapezoidal load wave form (1-minute hold time), for plate in H 1100 condition (Ref. 28)

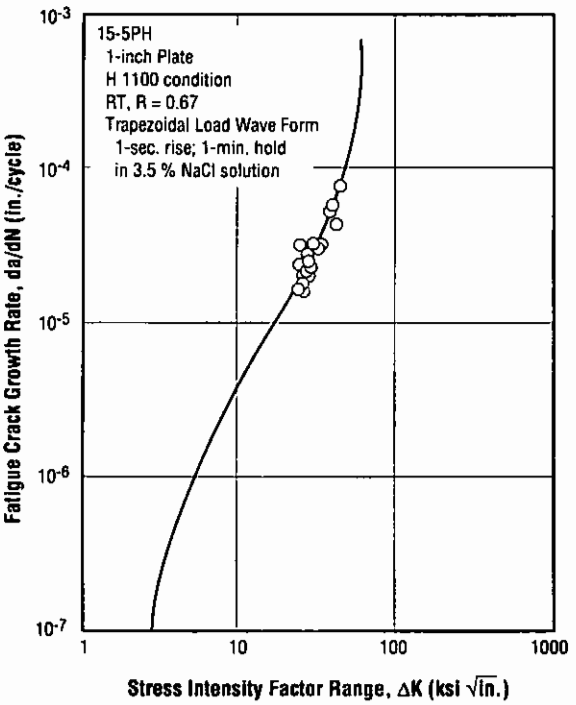

Figure 3.5.3.7 Room temperature fatigue crack growth rate in 3.5 percent NaCl solution at R = 0.67, trapezoidal load wave form (1-minute hold time), for plate in H 1100 condition (Ref. 28)

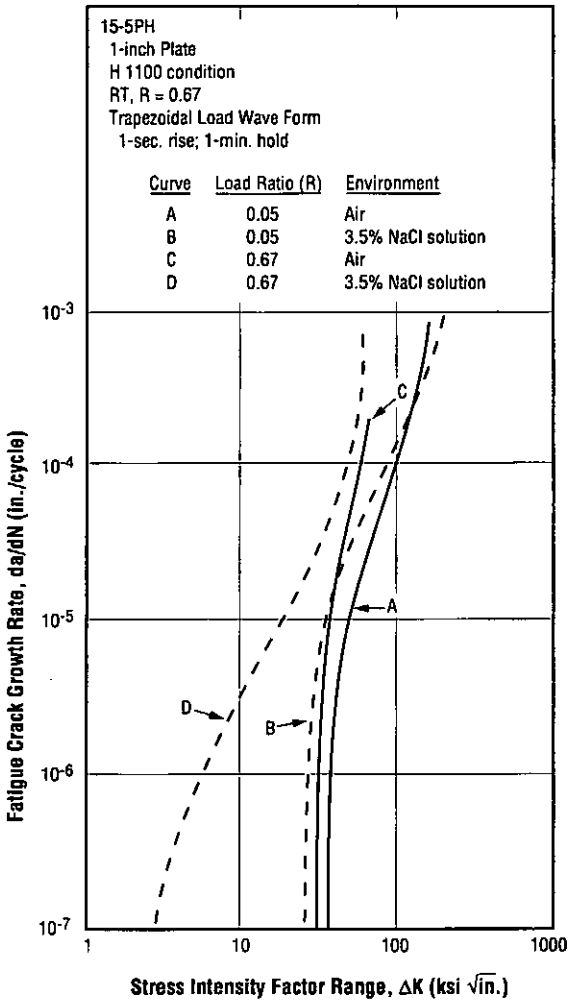

Figure 3.5.3.8 Effects of load ratio (R) and environment (air versus salt water) on room temperature fatigue crack growth rate for plate in H 1100 condition (Ref. 28)

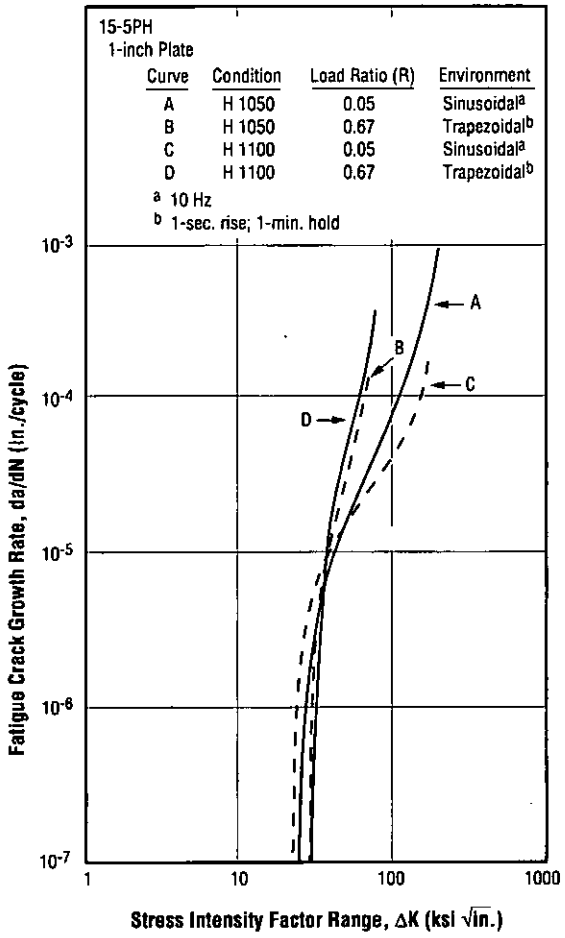

Figure 3.5.3.9 Effects of load wave form (sinusoidal versus trapezoidal), load ratio (R), and heat treated condition (H) on room temperature fatigue crack growth rate for plate (Ref. 28)

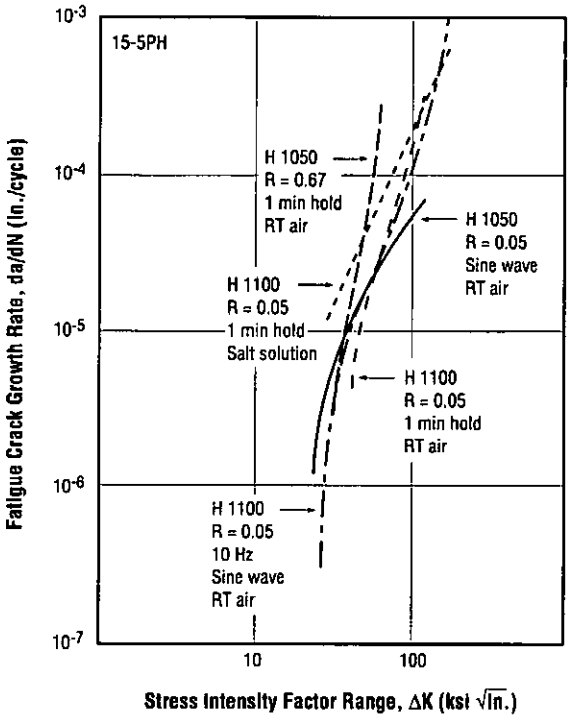

Figure 3.5.3.10 Fatigue crack growth rate in air and 3.5 percent aqueous NaCl solution for the H 1050 and H 1100 conditions (Ref. 51)

Table 3.6.2.1 Elastic moduli in tension and in torsion (Refs. 1, 7, 27)

Alloy	15-5PH			
Condition	H 900	H 1025	H 1075	H 1150
E (10^6 psi)	28.5	—	—	—
G[a] (10^6 psi)	11.2	11.0	10.0	10.0

[a] 17-4PH data, not expected to be different for 15-5PH.

Each value average duplicate tests from single heat.

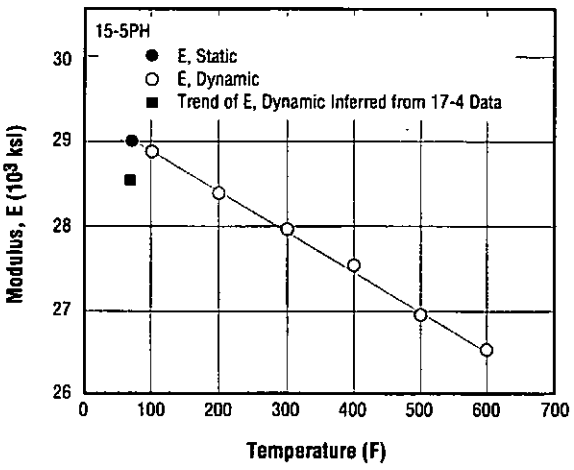

Figure 3.6.2.2 Effect of temperature on modulus of elasticity (Ref. 1)

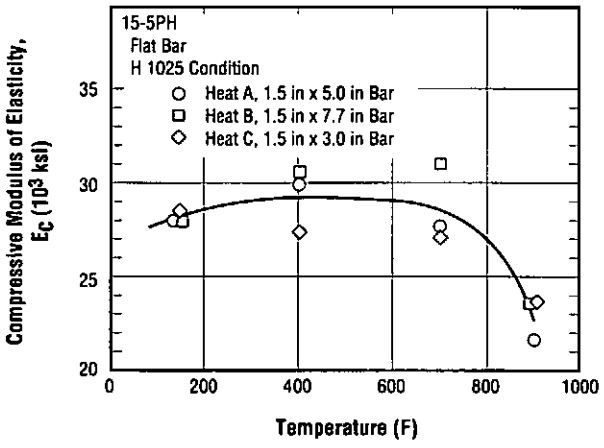

Figure 3.6.2.3 Effect of temperature on modulus of elasticity in compression of bar in H 1025 condition (Ref. 65)

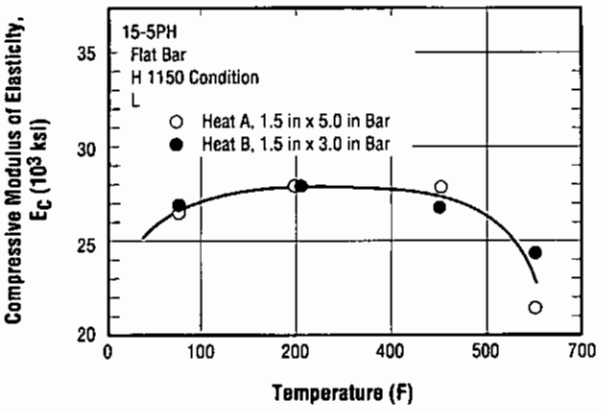

Figure 3.6.2.4 Effect of temperature on modulus of elasticity in compression of bar in H 1150 condition (Ref. 65)

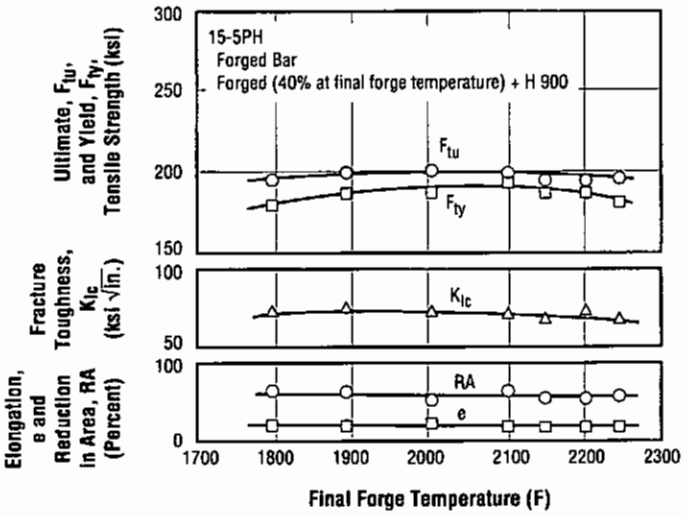

Figure 4.1.1.1 Influence of final forge temperature on tensile properties and plane strain fracture toughness (Ref. 39)

Table 4.1.4 Minimum room temperature bend radii (Ref. 27)

Alloy	15-5PH	
Form	0.090-inch Sheet	
Condition	Direction	Minimum Bend Radii
A	L	2t
	T	4t
H 900	L	3t
	T	5t
H 925	L	3t
	T	—
H 1025	L	3t
	T	
H 1150	L	2t
	T	
H 1150-M	L	2t
	T	

Average two heats.

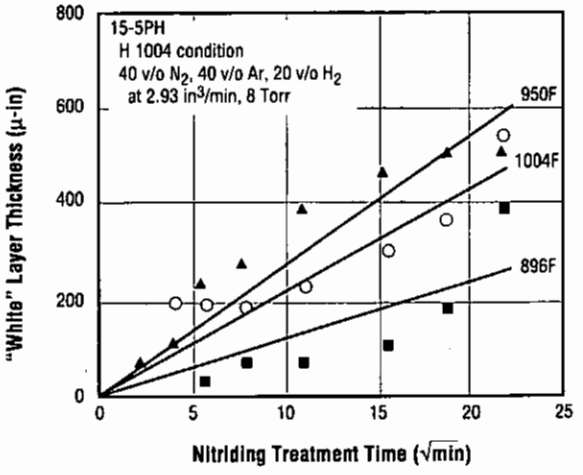

Figure 4.4.4.1 Effect of nitriding treatment time on "white" layer thickness (Ref. 47)

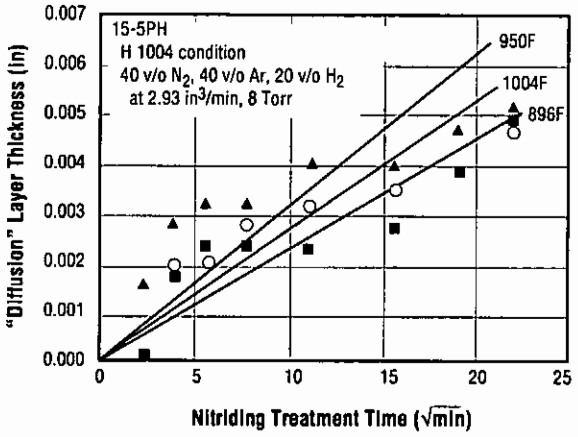

Figure 4.4.4.2 Effect of nitriding treatment time and temperature on "diffusion" layer thickness (Ref. 47)

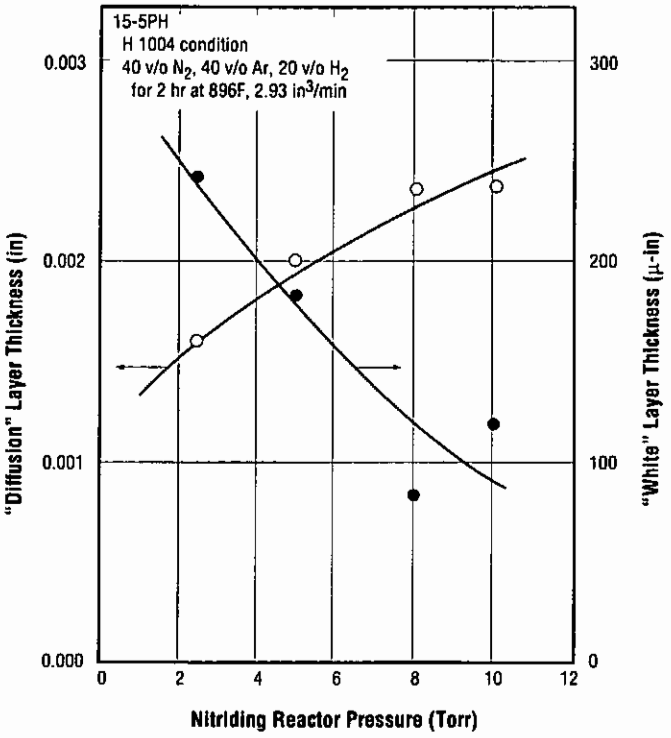

Figure 4.4.4.3 Effect of nitriding reactor pressure on "white" and "diffusion" layer thicknesses (Ref. 47)

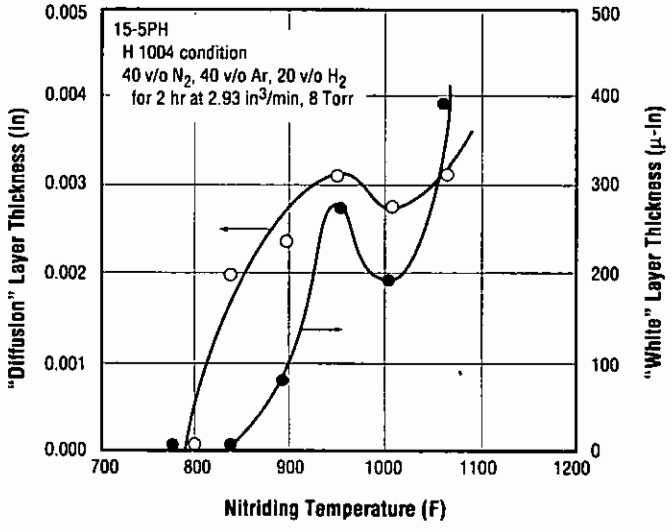

Figure 4.4.4.4 Effect of nitriding treatment temperature on thicknesses of "white" and "diffusion" layers (Ref. 47)

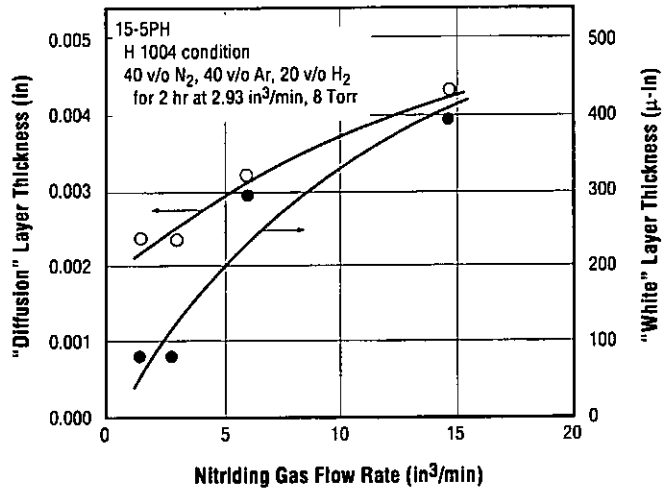

Figure 4.4.4.5 Effect of nitriding gas flow rate on "white" and "diffusion" layer thicknesses (Ref. 47)

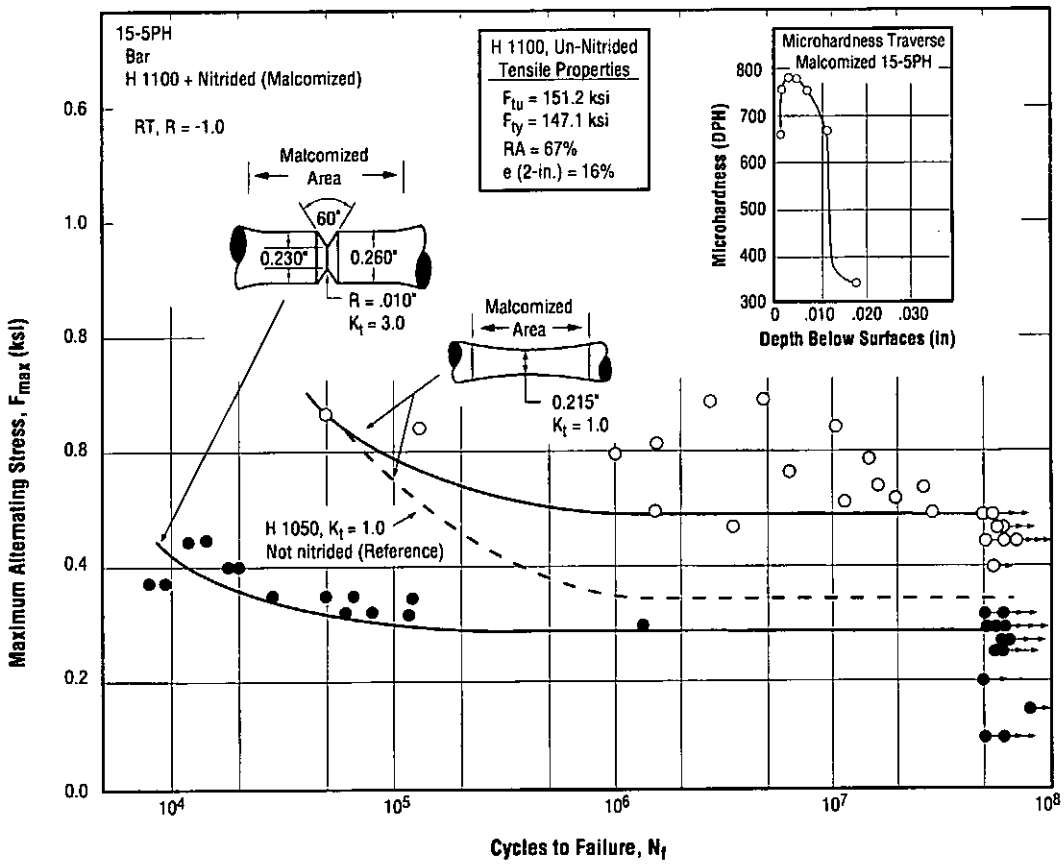

Figure 4.4.4.8 Smooth and mild-notch rotating beam fatigue strength of (proprietary Malcomizing) nitrided bar in H 1100 condition, with reference to smooth fatigue strength of bar not nitrided (Ref. 45)

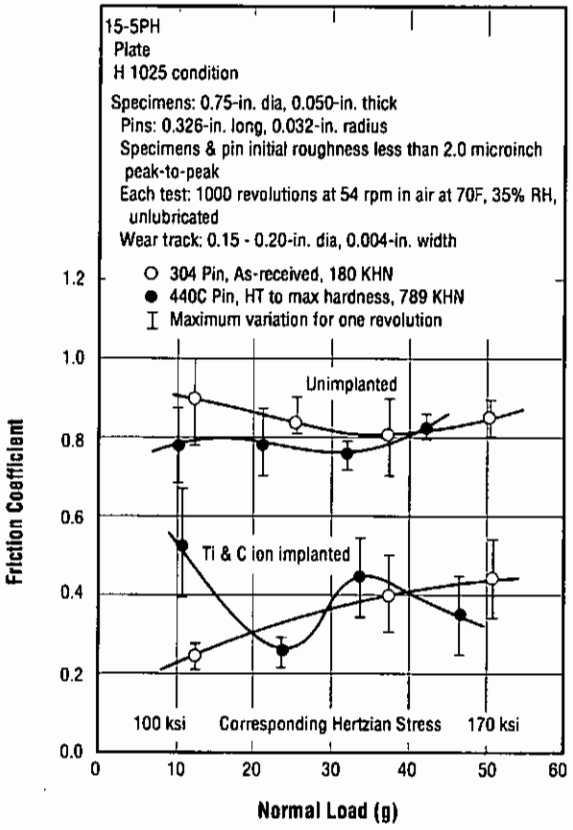

Figure 4.4.5.1 Influence of titanium and carbon ion implantation on unlubricated friction after 1000 pin-on-disc revolutions (Ref. 36)

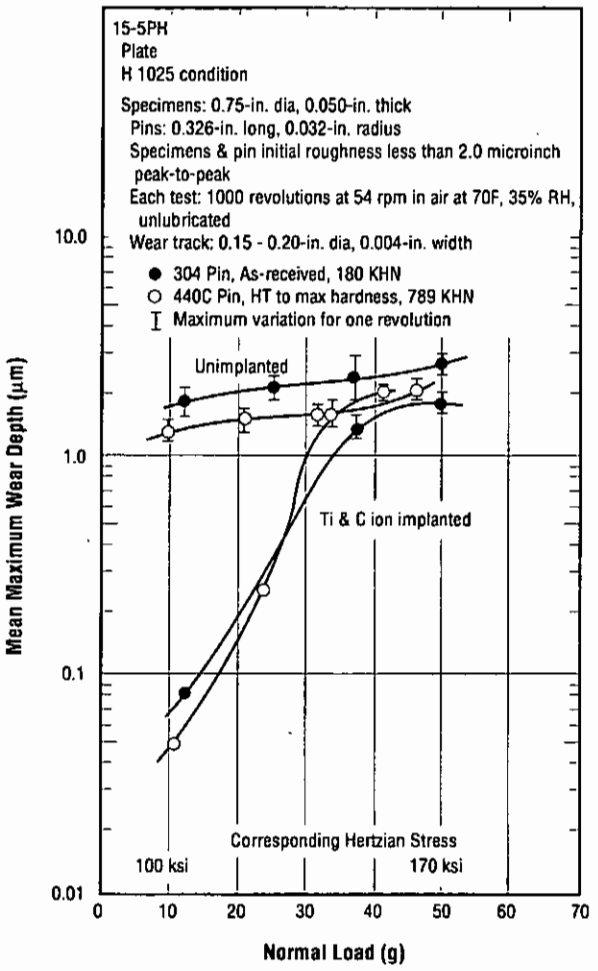

Figure 4.4.5.2 Influence of titanium and carbon ion implantation on unlubricated wear depth after 1000 pin-on-disc revolutions (Ref. 36)

[See ASTM Test Standard G 99-90 for Pin-on-Disk Wear Test Procedure]

Table 4.4.5.3 304 stainless steel pin wear in pin-on-disc tests of Ti and C ion implanted plates and of unimplanted plates (Ref. 36)

Alloy	15-5PH		
Form	Plate		
Condition	H 1025 + Ti & C Ion Implanted		
Pin Wear Scar Diameter (in)			
Normal Load (g)	Hertzian Stress (ksi)	Unimplanted	Ion Implanted
12.3	106	0.0066	< 0.0008
25.5	134	0.0115	< 0.0008
37.5	152	0.0123	0.0049
50.4	169	0.0094	0.0059

Specimens: 0.75-inch diameter, 0.050-inch thick.

Pins: 0.326-inch long, 0.032-inch radius.

Specimen and pin initial roughness < 2.0 μ-inch peak-to-peak.

Each test: 1000 revolutions @ 54 rpm in air at 70F, 33% RH, unlubricated.

Wear track: 0.15 - 0.20-inch diameter, 0.004-inch width.

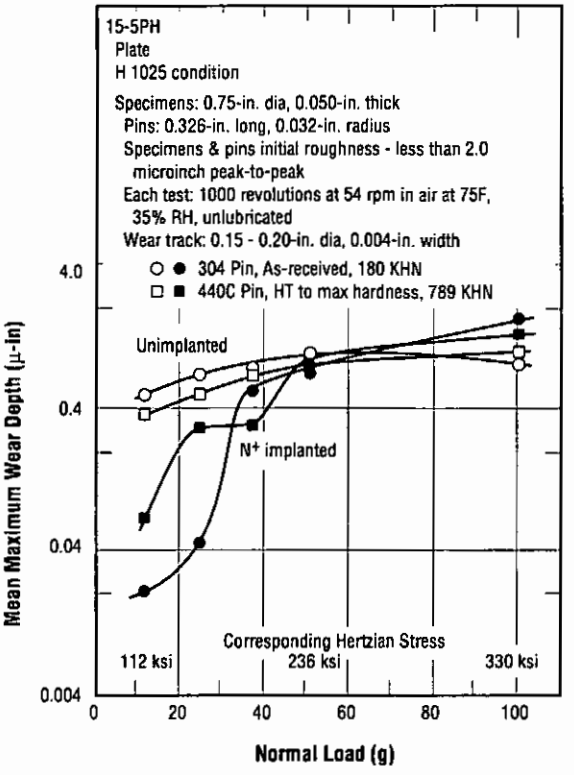

Figure 4.4.5.4 Influence of N^+ implantation on unlubricated wear depth after 1000 pin-on-disc revolutions (Ref. 38)

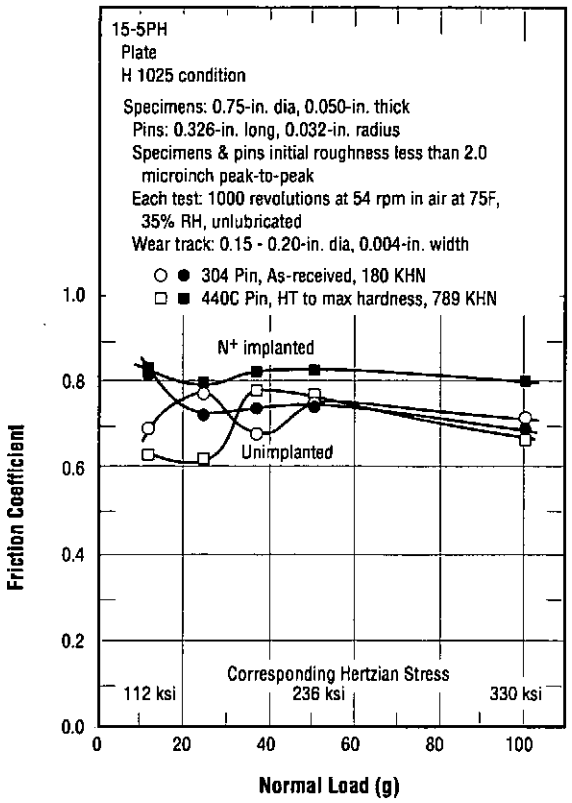

Figure 4.4.5.5 Influence of N^+ implantation on unlubricated friction after 1000 pin-on-disc revolutions (Ref. 38)

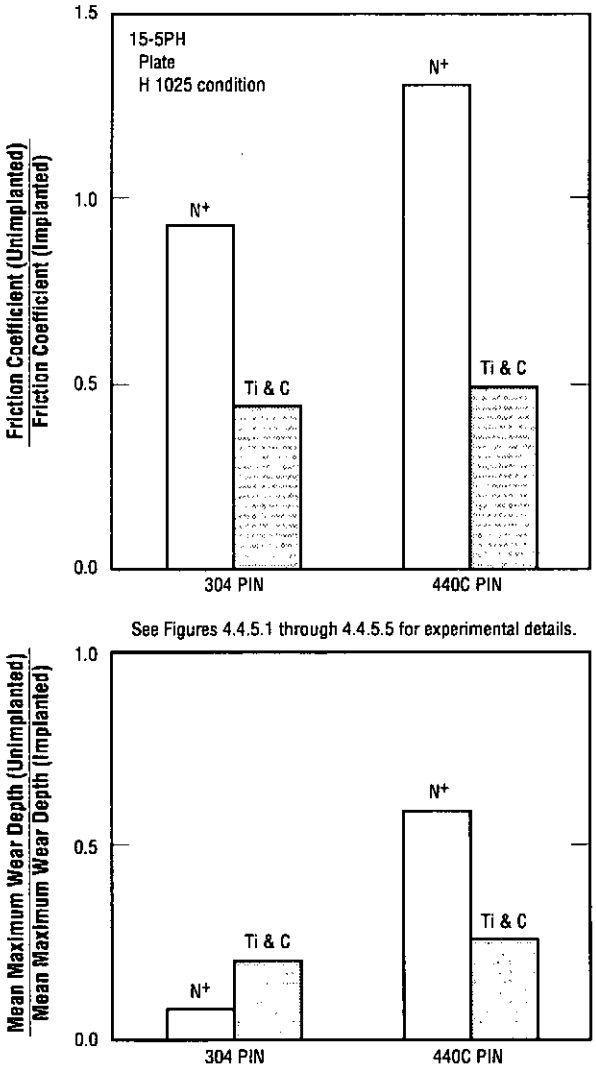

See Figures 4.4.5.1 through 4.4.5.5 for experimental details.

Figure 4.4.5.6 Influence on ion implantation (Ti and C or N^+) on unlubricated friction coefficient and mean maximum wear depth at 173 ksi Hertzian stress, expressed as ratios of unimplanted to implanted values (Ref. 38)

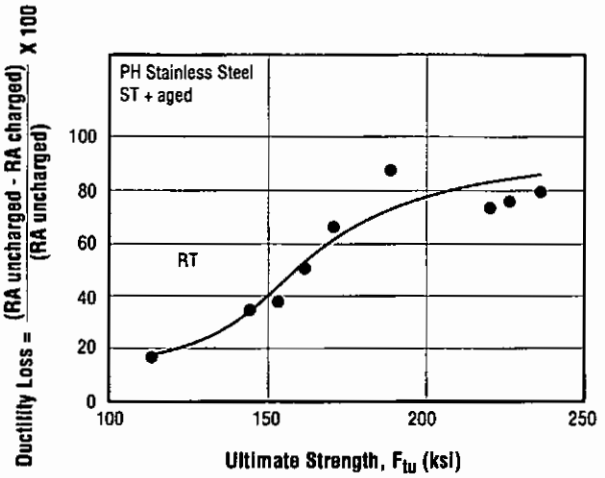

Figure 4.4.6.1 Effect of strength on ductility loss for typical PH steel specimens hydrogen charged at 90A/m^2 and tensile tested at room temperature (Ref. 33)

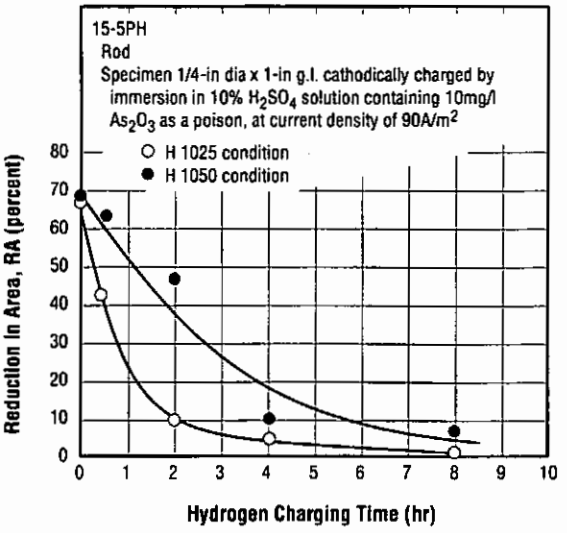

Figure 4.4.6.2 Effect of hydrogen charging on ductility of rod in H 1025 and H 1050 conditions (Ref. 57)

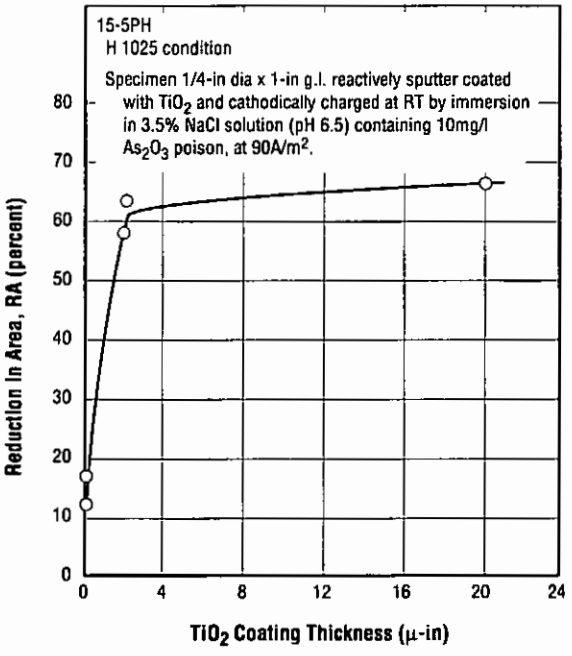

Figure 4.4.6.3 Effect of TiO_2 film thickness on ductility of specimens hydrogen charged for four hours at 90A/m^2 and tensile tested at room temperature (Ref. 52)

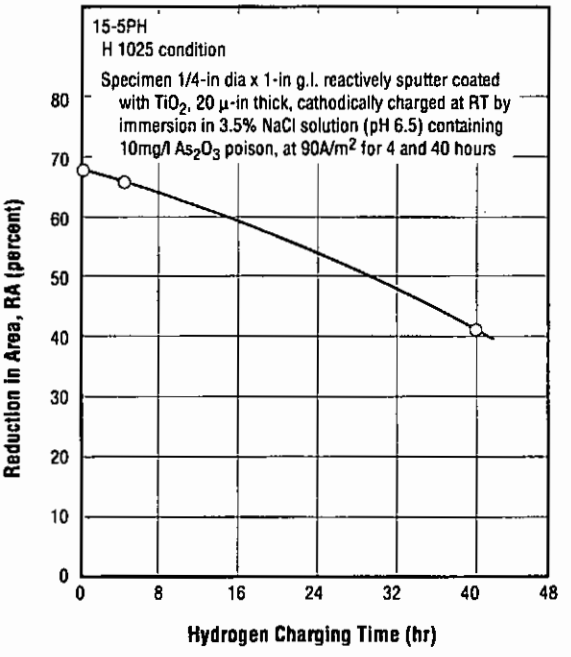

Figure 4.4.6.4 Effect of hydrogen charging time on ductility of TiO_2 coated (20 μ-in thick) specimens (H 1025 condition) tensile tested at room temperature after charging. (Ref. 52)

REFERENCES

1. Armco 15-5PH Precipitation-Hardening Stainless Steel Bar and Wire, *Armco Product Data Bulletin S-21a*, Armco Steel Corporation, Middletown, Ohio, (March 1968).
2. W.C. Clarke, Jr., "Applications and Properties of 15-5PH," *Metal Progress*, pp. 93 to 96, (August 1967).
3. W.C. Clarke, Jr. and H.W. Garvin, "Effect of Composition and Section Size on Mechanical Properties of Some Precipitation-Hardening Stainless Steels," American Society for Testing and Materials, *Special Technical Publication No. 369* (1965).
4. "Selection Guide - Armco Precipitation-Hardening Stainless Steel," Armco Steel Corporation, Middletown, OH.
5. Aerospace Material Specification, AMS 5658C, (July 1, 1976). (Superceded by Ref. 6)
6. Aerospace Material Specification, AMS 5659H, (March, 1995).
7. A.F. Hoenie and D.B. Roach, "New Developments in High Strength Stainless Steels," *DMIC Report 223*, Defense Metals Information Center, Battelle Memorial Institute, Columbus, OH (January 3, 1966).
8. R.J. Nekervis, C.H. Lund and A.M. Hall, "Status of High-Strength Steels for the Aircraft Industry," TML Report No. 91, Titanium Metallurgical Laboratory, Battelle Memorial Institute, Columbus, OH (January 3, 1958).
9. "Casting Armco 17-4PH and 15-5PH Precipitation-Hardening Stainless Steels," *Armco Products Data Bulletin SF-3*, Armco Steel Corporation, Middletown, Ohio (November, 1967)
10. R.E. Palmer and E.G. Takacs, "Magnetic Properties of Armco 17-4PH," Armco Steel Corporation, Baltimore, MD (October 31, 1967)
11. W. C. Clark, Jr., "A Study of Embrittlement of a Precipitation-Hardening Stainless Steel and Some Related Materials," Armco Steel Corporation, Baltimore, MD.
12. Private Communication with H. W. Garvin, Senior Research Engineer, Armco Steel Corporation, Baltimore, MD.
13. Aerospace Material Specification, AMS 5346A, (01 April 1993).
14. Aerospace Material Specification, AMS 5347, (16 October 1978).
15. Aerospace Material Specification, AMS 5356 (16 October 1978).
16. Aerospace Material Specification, AMS 5357 (16 October 1978).
17. Aerospace Material Specification, AMS 5400 (15 January 1979).
18. Aerospace Material Specification, AMS 5348A (01 January 1985).
19. Aerospace Material Specification, AMS 5862D (01 January 1991).
20. Aerospace Material Specification, AMS 5825E (01 October 1992).
21. Aerospace Material Specification, AMS 5826D (April 1994).
22. Aerospace Material Specification, AMS 5827D (01 October 1992).
23. American Society for Testing and Materials, ASTM A 693-93(XM-12) (15 July 1993).
24. American Society for Testing and Materials, ASTM A 564/A 564M-95(XM-12) (15 January 1995).
25. American Society for Testing and Materials, ASTM A 705/A 705M-95(XM-12) (15 January 1995).
26. R.M. Nagan and R.J. Cunningham, "Optimizing Fatigue Properties of Cast 15-5PH Steel," *Metal Progress*, Vol. 119, No. 4, pp 72-77 (March 1981).
27. "Armco 15-5PH Precipitation-Hardening Stainless Steel Sheet and Strip," *Armco Product Data Bulletin S-21a*, Armco Steel Corporation, Middletown, OH (1994).
28. K.R. Kondas, "Influence of Microstructure and Load Wave Form Control on Fatigue Crack Growth Behavior of Precipitation Hardening Stainless Steels," PhD Thesis, University of Missouri-Columbia (July 1976).
29. G.V. Smith, "Evaluation of the Elevated Temperature Tensile and Creep Rupture Properties of 12 to 27 Percent Chromium Steels," ASTM Data Series Publication DS 59.
30. J.E. Mortland, R.M. Evans, and R.E. Monroe, "Welding and Brazing of Precipitation-Hardening Stainless Steels," Prepared for NASA by Battelle Memorial Institute under Contract No. NASW-1948 (30 April 1970).
31. T. Allgeier and W.T. Evans, "Mechanical Hysteresis in Force Transducers Manufactured From Precipitation-Hardened Stainless Steel," Proceedings of the Institution of Mechanical Engineers, Part C: *Journal of Mechanical Engineering Science*, Vol. 209, No. C2 (1995).
32. "Mechanical Property Data - 15-5PH (H 1025) Stainless Steel Alloy: Hot-Rolled Plate," University of Dayton Report UDR-TM-84-14 on Contract No. F33615-82-C-5102 (May 1984).

33. G.T. Murray, "Prevention of Hydrogen Embrittlement by Surface Films," *Hydrogen Embrittlement: Prevention and Control*, ASTM STP 962, pp. 304-317 (1988).

34. M.J. Cieslak, "Hot-Cracking Mechanism in CO_2 Laser Beam Welds of Dissimilar Metals Involving PH Martensitic Stainless Steels," *Welding Research Supplement*, pp. 57s-60s (February 1987).

35. W.C. Clark, Jr., "A Study of Embrittlement of a Precipitation-Hardening Stainless Steel and Some Related Materials," *Transactions of the Metallurgical Society of AIME*, Vol. 245, pp. 2135-2140 (October 1969).

36. L.E. Pope, F.G. Yost, D.M. Follstaedt, J.A. Knapp, and S.T. Picraux, "Effects of Ion Implantation on Friction and Wear of Stainless Steels," Sandia National Labs Report No. SAND-82-0979C/CONF-820483-1, presented at Wear of Materials Conference, Reston, VA (11 April 1982).

37. D.M. Follstaedt, F.G. Yost, and L.E. Pope, "Microstructure of Stainless Steels Exhibiting Reduced Friction and Wear After Implantation with Ti and C," Sandia National Labs Report No. SAND-83-1234C/CONF-820483-13, presented at Materials Research Society Annual Meeting, Boston, MA (14 November 1983).

38. F.G. Yost, S.T. Picraux, D.M. Follstaedt, L.E. Pope, and J.A. Knapp, "The Effects of N^+ Implantation on the Wear and Friction of Type 304 and 15-5PH Stainless Steels," *Thin Solid Films*, Vol. 107:3, pp. 287-295 (23 September 1983).

39. G.W. Kuhlman, R. Pishko, W.S. Darden, and W.L. Krubsack, "Optimizing Mechanical Properties of Specialty, Stainless, and Heat-Resistant Alloy Steel Forgings by Thermomechanical Procesing," ASTM STP No. 903, *Steel Forgings*; Conference held Williamsburg, VA (28-30 November 1984).

40. Private communication between E.G. Takacs of Armco Steel Corporation, Baltimore, MD and J.E. Campbell, Battelle Memorial Institute, Columbus, OH (18 October 1972).

41. H. Espy, "Welding the PH Grades," Armoco Steel Corporation, Middletown, OH.

42. R.L. Rice, "Fracture Toughness and Fatigue Crack Propagation in 15-5PH Stainless Steel Bar," Memorandum from R.L. Rice to J.E. Campbell, Battelle Memorial Institute, Columbus, OH (31 January 1975).

43. T.J. Bosworth and A.J. Zvanut, "Development of a Direct Aging Filler Metal for Welding 15-5PH/17-4PH Steel," *Welding Research Supplement* (Supplement to the Welding Journal), pp. 159s-170s (June 1977).

44. C. Calabrese, "Fracture Mode and Toughness vs Temperature (-20 - 22C) for UNS-S15500 (15-5PH) Stainless Steel," *Engineering Fracture Mechanics*, Vol. 11:3, pp. 537-546 (1979).

45. M. Raefsky, "Metalurgical and Fatigue Evaluation of Malcomized 15-5PH Steel (AMS 5659B)," Boeing Company Engineering Materials Laboratory Report No. 69-378 (February 1970).

46. H. Garvin, "Casting 15-5PH and 17-4PH Stainless Steels," Armco Steel Corporation.

47. A. Cohen, M. Boas, and A. Rosen, "The Influence of Ion Nitriding Parameters on the Hardness Layer of 15-5PH Stainless Steel," *Thin Solid Films*, Vol. 141, No. 1, pp. 53-58 (15 July 1986).

48. J.H. Underwood, R.A. Farrara, G.P. O-Hara, J.J. Zalinka, and J.R. Senick, "Fracture Toughness and Fatigue Crack Initiation of Welded Precipitation-Hardening Stainless Steel," *Elastic-Plastic Fracture Test Methods: The User's Experience* (Second Volume), ASTM STP 1114, pp. 197-212 (1991).

49. C.W. Marschall and A.M. Hall, "Thermal and Mechanical Treatment for Precipitation-Hardening Stainless Steels," NASA Special Report on Contact NASW-1948 with Battelle Memorial Institute, Columbus, OH (30 April 1970).

50. D.E. Strohecker, A.F. Gerds, C.T. Olofsen, and F.W. Boulger, "Deformation Processing of Precipitation-Hardenable Stainless Steel," NASA Special Report on Contact NASW-1948 with Battelle Memorial Institute, Columbus, OH (01 May 1970).

51. J.E. Campbell, *Applications of Fracture Mechanics for Selection of Metallic Structural Materials*, Chapter 5: Fracture Properties of Wrought Stainless Steels, pp. 105-167, American Society for Metals, Metals Park, OH (1982).

52. J.G. Nelson and G.T. Murray, "Prevention of Hydrogen Embrittlement by a TiO_2 Surface Layer, *Metallurgical Transactions A*, Vol. 15A, pp. 597-600 (March 1984).

53. Y. Asayama, "Precipitation Processes and Notch Tensile Strengths of Precipitation Hardening Stainless Steels," *Journal of the Institute of Metals*, Vol. 45:7, pp. 731-739 (July 1981).

54. H.R. Habibi Bajuirani, C. Servant, and G. Cizron, "TEM Investigation of Precipitation Phenomena Occuring in PH 15-5 Alloy," *Acta Metall. Mater.*, Vol. 45(5), pp. 1613-1623 (1993).

55. *Military Handbook: Metallic Materials and Elements for Aerospace Vehicle Structures*, MIL-HDBK-5F, pp. 2-149 - 2-162 (01 November 1990).

56. *Products Bulletin S-6*, Armco Steel Corporation, Middletown, OH furnished by private communication with Kirk W. Olsen, Lord Corporation, Erie, PA (17 January 1997).

57. G.T. Murray, "Hydrogen Embrittlement of 15-5PH Stainles Steels," *Metallurgical Transactions A*, Vol. 12A, pp. 2138-2141 (December 1981).

58. K. Ozybaysal and O.T. Inal, "Thermodynamics and Structure of Solidification in the Fusion Zone of CO_2 Laser Welds of 15-5PH Stainless Steel," *Materials Science and Engineering*, A130, pp. 205-217 (1990).

59. J. Murali, M.R. Louthan, Jr. and R.P. McNitt, "Influence of Hydrogen on Age-Hardening Processes in 15-5 Precipitation Hardened Stainless Steel," Proceedings of Symposium MICON 78: *Optimization of Processing, Properties, and Service Performance Through Microstructural Control*, Houston, TX, published by ASTM, pp. 382-392 (April 1978).

60. T.S. Humphries and E.E. Nelson, "Stress Corrosion Cracking Evaluation of Martensitic Precipitation Hardening Stainless Steels," NASA TM-78257, NASA George C. Marshall Space Flight Center, Huntsville, AL (January 1980).

61. T.S. Humphries and E.E. Nelson, "Stress Corrosion Cracking Evaluation of Martensitic Precipitation Hardening Stainless Steels," NASA TM-53910, NASA George C. Marshall Space Flight Center, Huntsville, AL (12 September 1969).

62. R.R. Gaugh, "Sulfide Stress Cracking of Precipitation Hardening Stainless Steels," *Materials Performance*, Vol. 16:9, pp. 24-29 (September 1977).

63. R.R. Gaugh, "Stress Corrosion Cracking of Precipitation-Hardening Stainless Steels," *Materials Performance*, pp. 29-34 (February 1987).

64. C.S. Carter, D.G. Farwick, A.M. Ross and J.M. Uchida, "Stress Corrosion Properties of High Strength Precipitation Hardening Stainless Steels," *Corrosion*, Vol. 27:5, pp. 190-197 (May 1971).

65. P.E. Ruff and S.H. Smith,"Development of MIL-HNBK-5 Design Allowable Properties and Fatigue-Crack-Propagation Data for Several Aerospace Materials," AFML-TR-77-162 (October 1977).

66. *Structural Alloys Handbook*, published by CINDAS/ Purdue University, 1293 Potter Engineering Center, Room 316B, West Lafayette, IN 47907-1293 (1995).

Reference not used:

F. Bellucci, "Galvanic Corrosion Between Nonmetallic Composites and Metals: 1 - Effect of Metal and of Temperature," *Corrosion*, Vol. 47, No.10 (October 1991).